applied sciences

MDPI

Article

Computational Model and Constructal Design Applied to Thin Stiffened Plates Subjected to Elastoplastic Buckling Due to Combined Loading Conditions

Raí Lima Vieira [1], Guilherme Ribeiro Baumgardt [2], Elizaldo Domingues dos Santos [1,2], Luiz Alberto Oliveira Rocha [1,2], Thiago da Silveira [1], João Paulo Silva Lima [3] and Liércio André Isoldi [1,2,*]

[1] Graduate Program in Ocean Engineering, Federal University of Rio Grande, Rio Grande 96201-900, RS, Brazil; rai@furg.br (R.L.V.); elizaldosantos@furg.br (E.D.d.S.); luizrocha@furg.br (L.A.O.R.); thiagods@furg.br (T.d.S.)

[2] Graduate Program in Computational Modeling, Federal University of Rio Grande, Rio Grande 96201-900, RS, Brazil; guilherme.baumgardt@furg.br

[3] Department of Science and Technology, Federal University of Goiás, Goiania 74690-900, GO, Brazil; joaoplima@ufg.br

* Correspondence: liercioisoldi@furg.br

Featured Application: Numerical methodology to evaluate and optimize the geometry of stiffened plates submitted to elastoplastic buckling due to biaxial and lateral loading by means of the constructal design method.

Abstract: The size of ships has increased considerably in recent decades. This growth impacts the stress magnitude in the bottom hull plates, which constantly suffer from biaxial compression and lateral water pressure, potentially leading to buckling. Adding stiffeners is an effective alternative to increase mechanical buckling resistance if placed in a proper way. Several researchers have investigated the influence of stiffeners on plates under different loading conditions. However, the behavior under combined biaxial compression and lateral pressure has not yet been widely explored. This work aims to verify and validate a computational model to analyze the elastoplastic buckling of plates under biaxial compression and lateral pressure, applying it in a case study to define the ideal geometric configuration to increase ultimate buckling resistance, using the constructal design method and exhaustive search technique. In this study, a portion of the volume from a reference plate without stiffeners was converted into stiffeners to determine the optimal geometry for maximizing ultimate buckling resistance. The numerical model was verified and validated, and the case study identified the optimal plate configuration with five longitudinal and four transverse stiffeners, with a height-to-thickness ratio of 8.70, achieving a 284% increase in ultimate buckling resistance compared to the reference plate. These results highlight the importance of geometric evaluation in structural engineering problems.

Keywords: elastoplastic buckling; combined loadings; finite element method; constructal design; exhaustive search; ultimate strength

Academic Editors: Angelo Luongo and Simona Di Nino

Received: 22 February 2025
Revised: 8 March 2025
Accepted: 12 March 2025
Published: 19 March 2025

Citation: Vieira, R.L.; Baumgardt, G.R.; dos Santos, E.D.; Rocha, L.A.O.; da Silveira, T.; Lima, J.P.S.; Isoldi, L.A. Computational Model and Constructal Design Applied to Thin Stiffened Plates Subjected to Elastoplastic Buckling Due to Combined Loading Conditions. *Appl. Sci.* **2025**, *15*, 3354. https://doi.org/10.3390/app15063354

1. Introduction

In recent decades, the size of vessels has significantly increased to accommodate more containers, thereby reducing operational costs and enhancing the sustainability of the shipping process [1,2]. This growth in vessel dimensions has profound implications for the ship's structural components, particularly the hull's bottom panels, which are primarily composed of thin plates. These thin plates are subjected to various stress types, including tension, compression, bending, and torsion, due to their weight, the weight of the cargo, lateral water pressure, navigation forces, and sea conditions [3].

Due to their slenderness, thin plates inherently have low resistance to compressive loads. At the bottom of the hull, these plates are subjected to biaxial compressive stress and lateral water pressure [4]. This combined loading can lead to a phenomenon known as buckling, which initially occurs in the elastic regime, where the panel experiences instability and reversible deformation under a critical load. The buckling can transition to the elastoplastic regime, causing stress redistribution and developing a transverse tensile membrane, allowing the structures to support stress beyond critical strength without failure [5].

To mitigate this issue of buckling in thin plates, adding longitudinal and transverse stiffeners can significantly enhance their mechanical resistance. These stiffeners can support the weight of the cargo, in-plane loadings, and lateral water pressure [6]. In plates under longitudinal loading, the longitudinal stiffeners are responsible for carrying a portion of the longitudinal force applied to the plate, while the transverse stiffeners are used to subdivide the plate into smaller units [7]. The behavior is the opposite for plates under transverse loading, with the transverse stiffeners supporting the plate, and the perpendicular stiffeners subdividing the plate. For plates under biaxial loading, both longitudinal and transverse stiffeners perform both functions due to the application of longitudinal and transverse loadings. However, randomly adding stiffeners to non-stiffened plates does not efficiently improve resistance to buckling. Therefore, it is essential to understand how the geometric configuration of stiffened plates influences displacement and stress distribution, thus affecting their buckling resistance under different loading conditions.

In this context, the application of the constructal design method, developed by Adrian Bejan in 1996, emerges as an innovative solution. Bejan, when studying heat flow in cooling problems for electronic components, realized that the ideal solution resembled the structure of trees. This insight led him to formulate the constructal law, which states that for a finite system (natural or not) to persist, its configuration must evolve to facilitate flow [7,8]. This approach can also be applied to the buckling problem in plates, where evolving the system and facilitating flow means redistributing the displacement and stress to increase buckling resistance [9]. Recent studies have successfully applied the constructal design method to plates under different types of loading by reducing thickness and converting the corresponding volume into stiffeners, without adding materials, thus keeping the total material volume constant.

In addition, several researchers have investigated the influence of stiffened plate geometry in different loading scenarios, aiming to understand the mechanical behavior and improve its resistance.

Wang et al. [10] developed a novel methodology based on numerical buckling analyses to formulate empirical equations and design curves. This approach allows for predicting the maximum lateral pressure that stiffened panels under combined loading can withstand, considering various load scenarios, stiffener characteristics, and initial imperfections. The authors concluded that the position of the stiffeners significantly affects the ultimate strength, that considering local buckling as an initial imperfection provides more results of ultimate strength, and that the proposed design curves and empirical equations provide relatively high safety margins for reinforced plates concerning lateral pressure.

Baumgardt et al. [11] developed a computational model using the finite element method (FEM) in the ANSYS software (Version 2023R1) to simulate elastoplastic buckling in plates under uniaxial, biaxial, lateral, and combined compressive loading for different plate models. The authors concluded that the computational model could be used for elastoplastic buckling analysis under combined loads, as it was verified and validated, achieving differences of 2.47% and 4.83% compared to analytical and numerical reference results, and a maximum error of 5.40% compared to experimental results.

Ma et al. [12] experimentally and numerically studied the ultimate strength and collapse modes of stiffened plates subjected to biaxial compression and lateral pressure. The authors considered scenarios of loadings with and without lateral pressure, concluding that lateral pressure can reduce the ultimate buckling strength. However, when the deformation of the plate occurred in the direction opposite to the application of the lateral pressure, the lateral pressure resulted in an increase on the ultimate strength due to the restrained displacements.

Lima et al. [13] applied the constructal design method and exhaustive search technique to investigate the influence of longitudinal and transverse stiffeners, and their height-to-thickness ratio in a plate on buckling subjected to uniaxial compression. The authors considered two unstiffened plates with volumes V_{T1} and V_{T2} as ultimate stress reference and converted part of volume from plates into stiffeners, investigating different configurations regarding the number of stiffeners and height-to-thickness ratio. For the V_{T2} plate, the improvement in ultimate buckling resistance was 88.50% with the plate configuration using two longitudinal stiffeners and two transverse stiffeners. The difference between the best and worst configuration was 481.24%. For the V_{T1} plate, converting part of the steel volume into stiffeners was ineffective, achieving only a 7.38% improvement in ultimate buckling stress, reinforcing the importance of the geometry influence research.

Amaral et al. [14] also applied constructal design and exhaustive search to evaluate plates subjected to pure lateral load, ranging the number of longitudinal and transverse stiffeners. The authors concluded that plates with configuration using two longitudinal–five transverse stiffeners, and two longitudinal–six transverse stiffeners can efficiently reduce displacements and improve resistance in the proposed scenario. Improvement in displacements resulted in a 95.23% reduction compared to the reference plate, while bending resistance was increased by 44.98% compared to the reference plate. Just adding stiffeners to an unstiffened plate does not necessarily improve mechanical behavior.

Despite some studies applying constructal design in different scenarios of plate and stiffener geometries subjected to different types of loadings, it remains a challenge to find studies that fully understand how the geometric configuration of stiffeners impacts the buckling resistance and displacements of plates subjected to combined loading, such as biaxial compression and lateral pressure.

In this context and inspired by Lima et al. [13], the main goals of the present study are: (i) to develop a computational model in ANSYS Mechanical APDL to numerically simulate the mechanical behavior of plates under elastoplastic buckling subjected to biaxial compressive loading combined with lateral pressure; and (ii) to apply the developed computational model together with the constructal design method and exhaustive search technique in a case study. This approach will allow understanding how the variation in degrees of freedom affects the performance indicators and identifying the optimal configuration of stiffened plates that improve the ultimate buckling resistance in this loading scenario. To do so, taking a plate without stiffeners and its ultimate buckling stress as a reference, 30% of its steel volume is transformed into I-shaped longitudinal and transverse stiffeners. Additionally, the number of longitudinal and transverse stiffeners and their height-to-thickness ratio varies, generating several new geometric configurations with the same total volume of material. By numerically determining the ultimate buckling resistance of these new configurations, the best geometric configuration for the loading scenario under investigation can be identified.

It is important to mention that several optimization methods, such as those proposed by Liu et al. [15] and Amouzgar and Strömberg [16], focus on adaptive sampling and meta-modeling to efficiently determine optimal geometric configurations. While effective in reducing computational costs, these approaches may not fully capture the influence of geometric variations on structural performance. In contrast, the methodology applied in Lima et al. [13] and adopted in this study not only identifies the optimized geometry, but also provides insight into how degrees of freedom affect performance indicators. Constructal design systematically explores geometric configurations, while exhaustive search ensures a comprehensive comparison across all possibilities. This approach provides deeper insights into how geometry influences mechanical resistance, making it particularly suitable for problems where structural behavior is strongly dependent on geometric parameters, such as stiffened plates under elastoplastic buckling.

2. Materials and Methods

2.1. Computational Modeling of Buckling

The elastoplastic buckling analysis needs to consider initial imperfections. As in thin plates, the elastoplastic regime occurs after the elastic buckling; in this buckling model, the first buckling mode was considered as the basis for defining the imperfect initial configuration for the elastoplastic buckling computational model. So, for each elastoplastic analysis, a previous elastic buckling numerical simulation is necessary.

2.1.1. Computational Modeling of Elastic Buckling

The numerical modeling of elastic buckling considers an eigenvalue and eigenvector problem, with the smallest eigenvalue corresponding to the critical buckling load and the respective eigenvector representing the first buckling mode [17]. The numerical model is based on the analytical model described by Przemieniecki [18], in which the global matrix equation is:

$$[K]\,\{U\} = \{P\}, \tag{1}$$

where $\{U\}$ is the unknown displacement vector, $[K]$ is the stiffness matrix of the system, and P is the external loading vector. $[K]$ is composed of the geometric stiffness matrix $[K_G]$ and the conventional stiffness matrix for small deformations $[K_E]$:

$$[K] = [K_E] + [K_G], \tag{2}$$

being $[K_G]$ a function of the initial internal load vector $\{N_0\}$ of the material. When the load reaches a value equal to the reference load multiplied by an amplification factor, $[K]$ adjusts as follows:

$$[K] = [K_E] + \lambda[K_G], \tag{3}$$

where λ is an amplification factor (eigenvalue). Thus, the equilibrium of the elastic buckling problem results in:

$$[[K_E] + \lambda[K_G]]\,\{U\} = \lambda\{N_0\}, \tag{4}$$

with $\{U\}$ being obtained by:

$$\{U\} = [[K_E] + \lambda[K_G]]^{-1}\lambda\{N_0\}. \tag{5}$$

In the inverse matrix, the adjoint matrix is divided by the determinant of the coefficients, causing the displacements to tend toward infinity when:

$$\det[[K_E] + \lambda[K_G]] = 0. \tag{6}$$

The Lanczos method is used to determine the smallest λ, and the critical buckling load P_{cr} is then determined by:

$$P_{cr} = \lambda_1 \{N_0\} \quad (7)$$

where P_{cr} represents the critical load of elastic buckling, and the $\{U\}$ associated with this load defines the initial imperfections of the elastic buckling.

2.1.2. Computational Modeling of Elastoplastic Buckling

Although the elastoplastic buckling was defined with bilinear isotropic hardening, the material was considered as a linear elastic–perfectly plastic model, without strain-hardening, resulting in more conservative results. This regime involves the presence of geometric and material nonlinearities, causing $[K_G]$ and $\{U\}$ to no longer be proportional to the stresses. The initial imperfections of the elastic buckling were considered with the maximum amplitude value of initial imperfections [19]:

$$w_b = \frac{b}{2000} \quad (8)$$

where w_b is the maximum amplitude value of initial imperfections and b is the width of the plate. This maximum amplitude value multiplied to the first buckling mode displacements results in the initial shape of plate in the elastoplastic buckling, and it is considered in ANSYS, as described by Fonseca [20].

To determine the resultant displacements, two reference loads were defined as corresponding to the material's yield load for the plate and for the stiffeners:

$$P_{Rp} = \sigma_y t_p, \quad (9)$$

$$P_{Rs} = \sigma_y t_s, \quad (10)$$

where P_{Rp} represents the reference load of the plate, σ_y represents the yield stress of the material, t_p represents the plate thickness (or only t for an unstiffened plate), P_{Rs} represents the reference load of the stiffener, and t_s represents the stiffener thickness. The application of these reference loads ensures the application of the σ_y over the stiffened plate. The reference loads are divided into sub-steps and incremented with the Newton–Raphson iterative method, where the unbalanced load vector represents the difference between the external loads and the nonlinear internal forces at each iteration. At each iteration, the displacement vector was recalculated:

$$\{\varphi\}_{r+1} = \{P\}_{i+1} - \{N_{NL}\}_r, \quad (11)$$

$$\{\varphi\}_{r+1} = [\{K_T\}_r][\Delta U]_{r+1}, \quad (12)$$

$$\{\Delta U\}_{r+1} = \{U\}_r + \Delta U, \quad (13)$$

where $\{\varphi\}$ represents the unbalanced load vector, $\{P\}$ represents the vector of applied external forces, $\{N_{NL}\}$ represents the vector of nonlinear internal forces, $\{K_T\}$ represents the tangent stiffness matrix of the material, and ΔU represents the displacement increment vector needed to reach the equilibrium configuration.

The ultimate buckling load P_u and ultimate buckling stress σ_u were determined when, as the load sub-steps increments were applied, the material deformations reached magnitudes so large that the internal loads could no longer balance or meet the equilibrium tolerance, indicating that the material had reached its maximum stress [13].

For the case study, due to the higher number of simulations, the number of sub-steps was standardized according to the sub-steps convergence test realized before the simulations. To verify and validate the computational model of buckling, the number of sub-steps was set to 200, with a maximum of 400 and a minimum of 100. The solution convergence criteria were based on ANSYS's standards for force, moment, and displacements, i.e., a non-linear solution is considered converged when the normalized residual of any key variable (force, moment, or displacement) falls within an acceptable threshold. This occurs when the sum of the absolute values of the unbalanced residuals, whether in terms of force, moment, or displacement, is at most 0.5% of the corresponding applied or incremental quantity. In this context, the unbalanced residual represents the portion of the force, moment, or displacement that has not yet been balanced in the iterative process, while the reference value corresponds to the total applied or incremental quantity used for comparison.

2.1.3. Computational Model Discretization

SHELL finite elements were used to reduce the computational complexity of 3D analyses to 2D. By minimizing shear effects, which are negligible in thin plate behavior, these elements accurately determine the ultimate buckling stress for thin and moderately thick plate structures.

For complex nonlinear analyses, the SHELL281 finite element, recommended by ANSYS [21] and employed by Baumgardt et al. [11], was utilized in this computational model, due to its greater accuracy in nonlinear problems and in representing the effects of bending and plasticity. This eight-node element, with six degrees of freedom per node (translations and rotations in the x, y, and z axes), allows for the creation of quadrilateral or triangular elements. SHELL281 offers versatility through comprehensive configuration options, including adjustable integration point quantities for complex geometries, thickness offset, and advanced curved shell formulation. In this model, nine integration points were used along with the shell thickness. This choice, aligned with the ANSYS recommendation to use five or more points in simulations involving plasticity, ensures adequate representation of the material's nonlinear behavior. Additionally, result storage was configured for the top, bottom, and middle surfaces (KEYOPT (8) = 2), and the other element configurations were considered as standard value from ANSYS [21].

For the case study, the element size was standardized according to the mesh convergence test conducted prior to the numerical simulations, and the element size for verification and validation was determined based on the results of the mesh convergence test for each specific case.

2.2. Computational Modeling of Plates

For the unstiffened plate, the relevant material properties are the module of elasticity E, Poisson's ratio ν, and the yield stress σ_y; while the geometric parameters are the length a, width b, thickness t, and volume V_p (Figure 1a). For the stiffened plate, the material properties and geometric parameters of the plate remain unchanged, except for the nomenclature of the plate thickness, which is denoted as t_s instead of t. For the stiffeners, the relevant mechanical properties are also E, ν, and σ_y, but some additional dimensions are needed: height h_s, thickness t_s, height-to-thickness ratio h_s/t_s, number of longitudinal stiffeners N_{ls}, longitudinal stiffeners spacing S_{ls}, number of transverse stiffeners N_{ts}, transverse stiffeners spacing S_{ts}, and stiffeners volume V_s (Figure 1b). The length of the longitudinal stiffeners is the same as the plate, a, while the length of the transverse stiffeners is equal to the width of the plate, b.

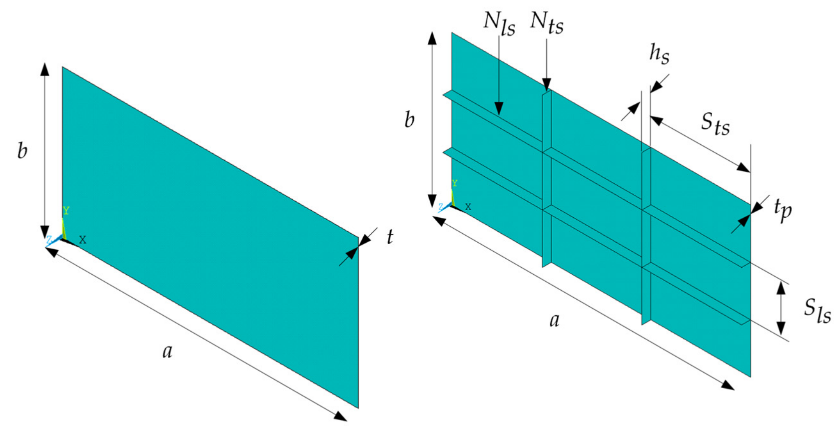

Figure 1. Computational modeling of: (**a**) unstiffened plate and (**b**) stiffened plate.

For the case study, the thickness offset of the SHELL281 finite element was the bottom one, which causes the plate's behavior to exhibit compressive stress and maximum U_z in the positive direction of the z axis, similarly to what occurs in the bottom plates of vessels during sagging, as illustrated by Wang et al. [10], as shown in Figure 2. Due to the selection of the bottom thickness offset, the height h_s of all stiffeners was increased by the value t_p to compensate for the overlap of the plate and stiffeners interface.

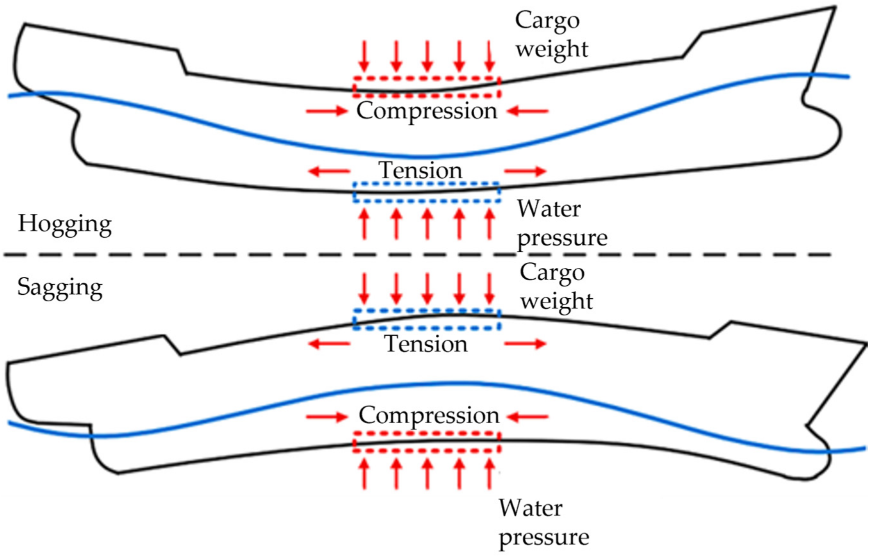

Figure 2. Behavior of vessel plates loading and deformations in sagging and hogging conditions (adapted from Wang et al. [10]), being the cargo weight the total weight that the ship is transporting and the continuous blue line the waterline.

2.2.1. Boundary Conditions

The stiffened plates used in constructing ship's hull are welded to adjacent sheets and stiffeners, being considered fixed in the boundary. However, representing the plate as simply supported results in a more conservative analysis of the plates' buckling resistance [19,22]. For this reason, all simulations consider simply supported plates, restricting out-of-plane displacements U_z along all the edges of the plate and stiffeners. Additionally, restrictions on both horizontal U_x and vertical U_y displacements are also applied, as shown in Figure 3.

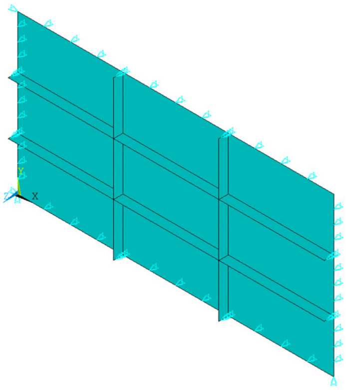

Figure 3. Boundary conditions of a simply supported stiffened plate, with displacement restrictions represented in blue on the stiffened plate boards, according to the respective axis directions.

2.2.2. Loading Application

For the case study, only horizontal P_x and vertical P_y in plane loadings were applied to the elastic buckling analysis. In the elastoplastic buckling analysis were applied the combined loading, which includes the P_x, P_y, and lateral pressure P_z. The values of P_x and P_y were the reference loading (Equations (9) and (10)), and the P_z module was constant and equal to 0.16 MPa, representing the extreme pressure conditions projected for a 100,000-ton class double-hull oil tanker [23]. First, the lateral pressure P_z is applied, and large deformations are obtained. After this, P_z is maintained, and biaxial loading is then applied.

2.3. Constructal Design Method and Exhaustive Search Technique

As in Lima et al. [13], the application of constructal design starts from an unstiffened plate that is considered as a reference, and its ultimate buckling strength σ_{uR} is adopted as a comparison parameter. The a and b were maintained constantly, and t was reduced to t_p to allocate volume for the stiffeners according to a defined volume fraction ϕ, as follows:

$$\phi = \frac{V_s}{V_p} = \frac{N_{ls}(a\,h_s t_s) + N_{ts}(b - N_{ls} t_s) h_s t_s)}{abt}, \tag{14}$$

where ϕ represents the fraction of the total volume of the reference plate that is transformed into stiffeners, V_s is the total volume of stiffeners, and V_p is the total volume of the reference plate.

The number of stiffeners N_{ls} and N_{ts} and their respective h_s/t_s are degrees of freedom (DOF) necessary for the application of constructal design, generating new geometric configurations of stiffened plates. The σ_u results of these proposed geometries were obtained and evaluated numerically. It is important to emphasize that the h_s and t_s are variables, but in each new configuration generated, they had the same values for both longitudinal and transverse stiffeners. How N_{ls} and N_{ts} are degrees of freedom, to respect the symmetrical distribution of the stiffeners on the plate, the spacings between stiffeners were defined as:

$$S_{ls} = \frac{b}{N_{ls} + 1}, \tag{15}$$

$$S_{ts} = \frac{a}{N_{ts} + 1}, \tag{16}$$

where S_{ls} is the spacing between longitudinal stiffeners and S_{ts} is the spacing between transverse stiffeners.

To understand how the P_z and h_s/t_s impacts on σ_u, three conditions of lateral pressure were considered: an application of lateral pressure in a positive direction of the z-axis, in a negative direction of the z-axis, and null pressure. However, the optimized stiffened plate configurations were investigated only for the application of positive lateral pressure and biaxial compressive loading, being the unstiffened plate under this condition defined as the reference plate. This was adopted due to the desirable positive displacement over z-axis, similarly to sagging behavior (Figure 3). Because of this, its respective ultimate buckling stress reference σ_{uR} was considered for comparisons with the other plate geometries. To compare these results, the σ_u resulted from geometric configurations proposed by constructal design were dimensionless as normalized ultimate buckling strength σ_{uN}. This serves as the performance indicator, and is calculated as:

$$\sigma_{uN} = \frac{\sigma_u}{\sigma_{uR}}, \tag{17}$$

where σ_{uN} is the normalized ultimate buckling stress, σ_u is the ultimate buckling stress obtained from the varying DOF, and σ_{uR} is the ultimate buckling stress of the reference plate.

In turn, the constructal design method is applied according to the following steps, shown in Figure 4.

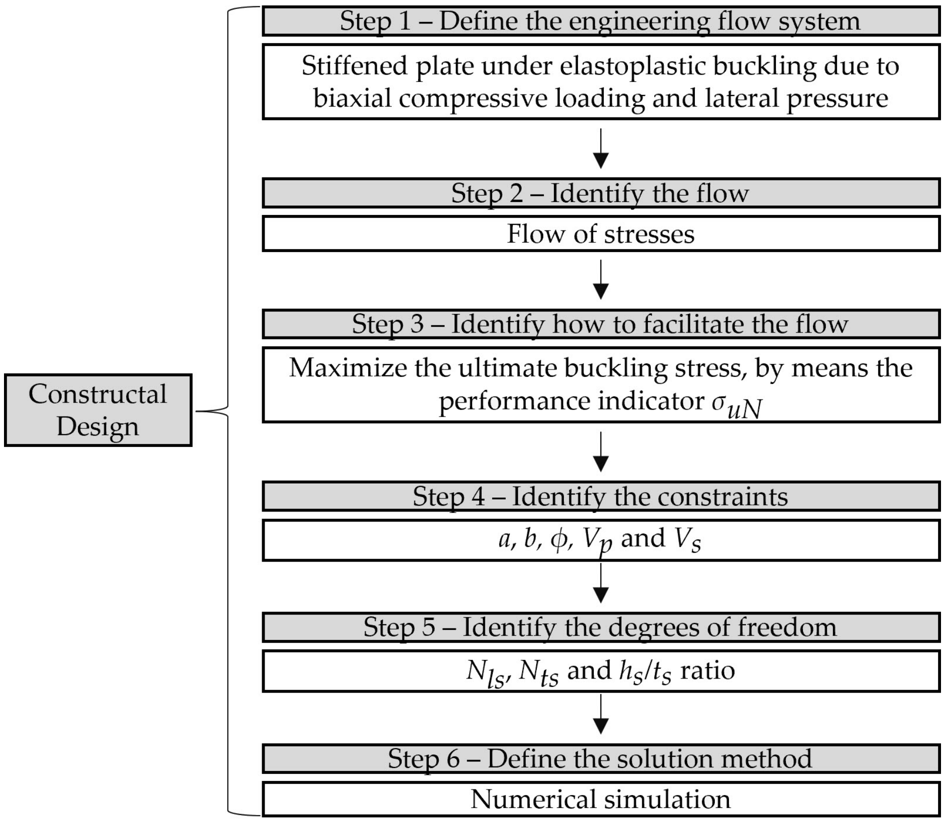

Figure 4. Steps of constructal design method (adapted from Lima et al. [13]).

The fraction ϕ was set as 0.3, identified by Lima et al. [13] as the best ratio between V_s and V_p to improve σ_u in elastoplastic buckling due to uniaxial compression, for a plate with the same dimensions considered in this study, with N_{ls} and N_{ts} values ranging from 2 to 5, resulting in sixteen plate configurations. While the t_s was defined as a minimum of 5 mm, set according to commercial dimensions, and varied incrementally up to 45 mm, and the h_s values range depending on the available volume, respecting the volume conservation. This resulted in eight different values of h_s/t_s for each plate configuration, leading to a total of 128 distinct stiffened plates geometries being investigated. As mentioned earlier, due the volume conservation, as N_{ls} and/or N_{ts} increase, the maximum h_s value that the stiffeners can achieve tends to decrease to respect this premise. Moreover, as t_s increases, the h_s value also tends to decrease due to the same principle. This behavior is common to all plate configurations and is illustrated in Figure 5, considering arbitrary N_{ls}, N_{ts}, and t_s values. Furthermore, the Supplementary Materials provides all the values of N_{ls}, N_{ts}, h_s, and t_s, which were determined through the application of constructal design and a graphical explanation of the influence of N_{ls}, N_{ts}, and t_s over h_s.

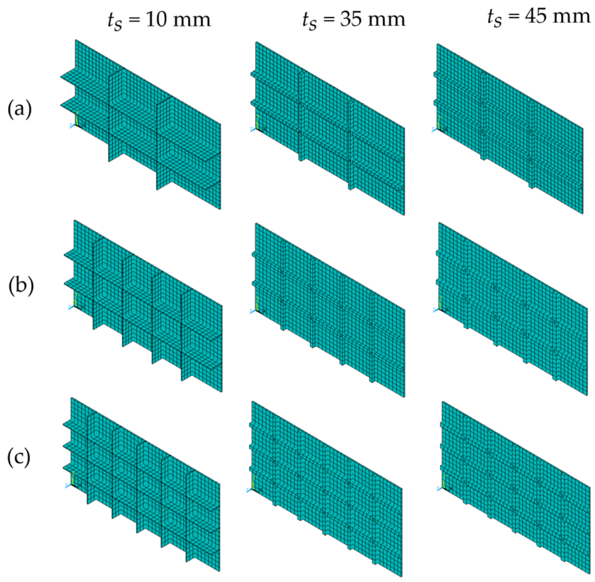

Figure 5. Influence of N_{ls}, N_{ts}, and t_s over h_s: (**a**) P(2;2), (**b**) P(2;4), and (**c**) P(3;5).

After that, the exhaustive search technique was applied, according to the subsequent steps shown in Figure 6.

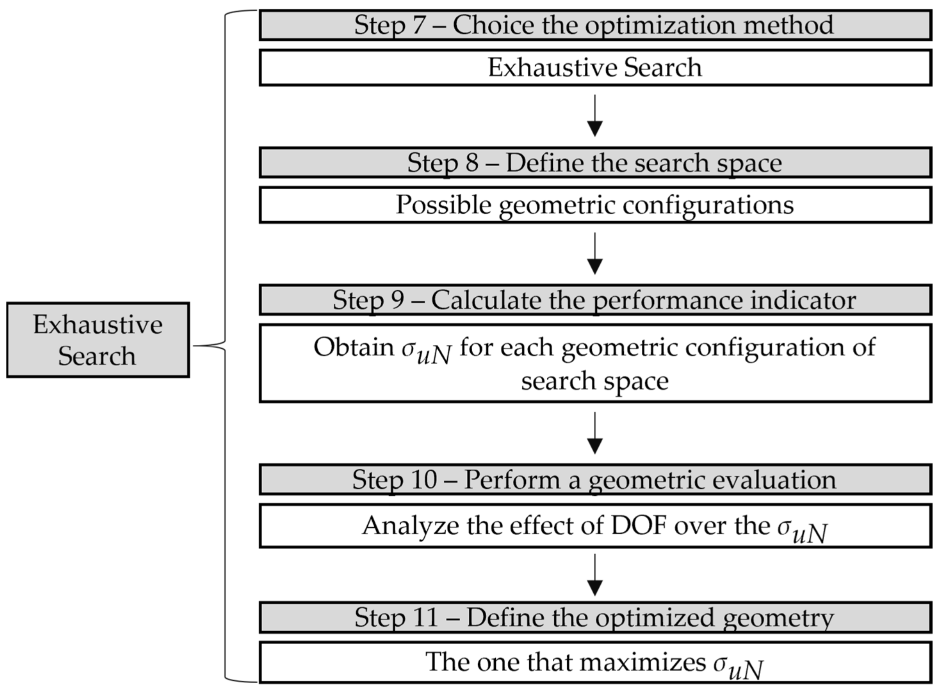

Figure 6. Steps of exhaustive search technique (adapted from Lima et al. [13]).

As earlier explained, the number of N_{ls} and N_{ts} ranging from 2 to 5, is allowed to generate sixteen different plate arrangements P(N_{ls}; N_{ts}): P(2;2), P(2;3), P(2;4), P(2;5), P(3;2), P(3;3), P(3;4), P(3;5), P(4;2), P(4;3), P(4;4), P(4;5), P(5;2), P(5;3), P(5;4), and P(5;5). By varying h_s/t_s for each arrangement, the optimal stiffened plate geometry was determined to enhance σ_{uN}. All these definitions formed the basis and sequence for the search space used to conduct the exhaustive search technique, as illustrated in Figure 7.

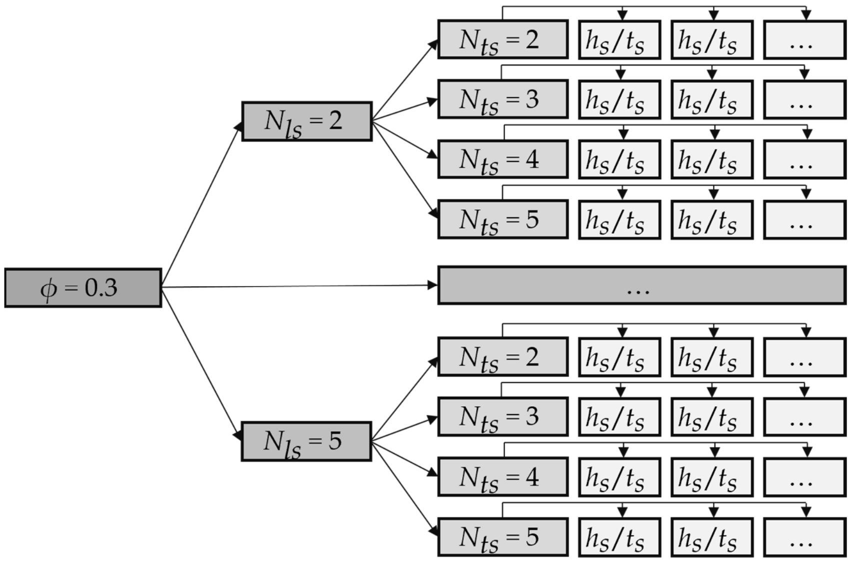

Figure 7. Search space sequence for exhaustive search technique application (adapted from Lima et al. [13]).

Through the variation of N_{ls}, N_{ts}, and h_s/t_s, and calculation of σ_{uN}, the h_s/t_s values were identified for each plate configuration that maximized the σ_{uN}. These values were defined as once optimized height-to-thickness $(h_s/t_s)_o$ and once maximized ultimate buckling strength $(\sigma_{uN})_m$. From these optimized and maximized values, the higher values of $(\sigma_{uN})_m$ and consequently their $(h_s/t_s)_o$ and N_{ts} were identified and defined as twice maximized ultimate buckling strength $(\sigma_{uN})_{mm}$, twice optimized height-to-thickness ratio $(h_s/t_s)_{oo}$, and once optimized number of transverse stiffeners $(N_{ts})_o$. Finally, from these last optimized and maximized values, the plate configuration with the highest ultimate strength was identified, being defined as the three times maximized ultimate strength $(\sigma_{uN})_{mmm}$, three times optimized $(h_s/t_s)_{ooo}$, twice optimized number of transversal stiffeners $(N_{ts})_{oo}$, and once optimized number of longitudinal stiffeners $(N_{ls})_o$.

3. Results and Discussion

3.1. Verification and Validation of Computational Modeling of Buckling

The verification and validation of computational buckling modeling were realized considering the critical and ultimate buckling stress of unstiffened and stiffened plates subjected to axial, biaxial, and combined loadings.

3.1.1. Verification of Elastoplastic Buckling Model Under Combined Loading on Unstiffened Plates

The first verification was carried out considering Paik and Seo [23]'s study, which applied longitudinal compressive loading σ_X and transverse compressive σ_Y loading in different ratios, and a constant lateral pressure P_z = 0.16 MPa to a simply supported unstiffened plate, with a = 4300 mm, b = 815 mm, t = 19 mm, E = 208.5 GPa, σ_y =315 MPa, and ν = 0.3. An initial imperfection of plate as $w_0 = b/200$, while the proposed model considered $w_0 = b/2000$ (Equation (8)). The geometry of the unstiffened plate with boundary conditions of the proposed model is shown in Figure 8.

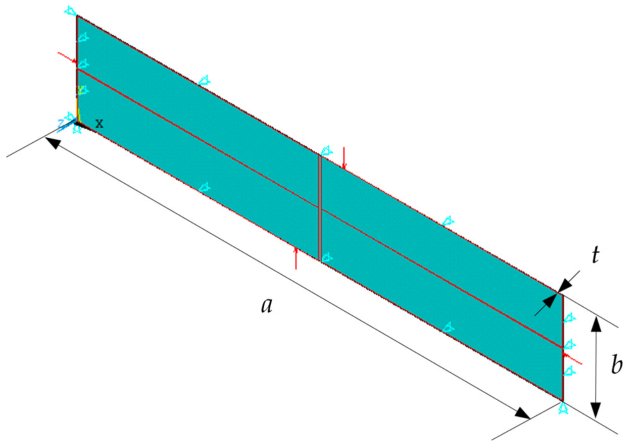

Figure 8. Unstiffened plate geometry and boundary conditions of the proposed model, with the blue symbols representing the displacement constraints according to the axis direction, the red arrows representing the biaxial compressive loading, and the red lines on the plate representing the applied lateral pressure.

The finite element size used in the proposed computational modeling was defined according to the mesh convergence test considering the loading condition σ_X : σ_Y = 0.8:0.2, as shown in Table 1.

Table 1. Mesh convergence test for verification of elastoplastic buckling model under combined loading on unstiffened plate.

Element Length (mm)	Number of Elements	σ_{uX} (MPa)
100	387	225.22
75	638	225.22
50	1462	225.22
25	5676	225.22

Considering the element size with 25 mm in Table 1, the proposed model resulted in σ_{uX} = 225.22 MPa and σ_{uY} = 56.30 MPa. When compared to the values obtained by Paik and Seo [23], which were σ_{uX} = 222.96 MPa and σ_{uY} = 55.72 MPa, the differences are 1.01% and 1.04% higher, respectively. For the ratio σ_X : σ_Y = 0.7:0.3, the proposed model resulted in σ_{uX} = 159.07 MPa and σ_{uY} = 68.17 MPa. When compared to the values obtained by Paik and Seo [23] which were σ_{uX} = 153.97 MPa and σ_{uY} = 65.99 MPa, the differences are 3.31% and 3.30% higher, respectively. Despite accounting for different boundary conditions and values of initial imperfections, the ultimate stress values confirm that the proposed model is verified for use in the elastoplastic analysis of unstiffened plates.

The second verification was performed considering Baumgardt et al.'s [11] work, which applied biaxial compressive loading and a constant lateral pressure P_z = 0.0507 MPa to a plate made of AH-36 steel, with a = 2000 mm, b = 1000 mm, t = 12 mm, E = 210 GPa, σ_y =355 MPa, and ν = 0.3, with a rectangular perforation in the center, with length a_0 =450 mm and width b_0 = 667 mm, as shown in Figure 9.

Baumgardt et al. [11] used the SHELL281 finite element with 30 mm and a quadrilateral form. The σ_u obtained with the proposed computational model was achieved according to the mesh convergence test shown in Table 2.

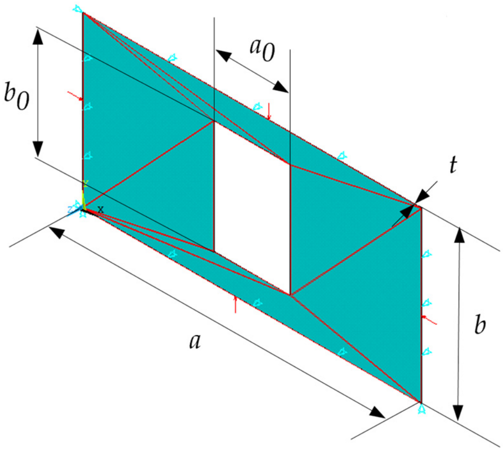

Figure 9. Unstiffened plate geometry with rectangular hole and boundary conditions of the proposed model, with the blue symbols representing the displacement constraints according to the axis direction, the red arrows representing the biaxial compressive loading, and the red lines on the plate representing the applied lateral pressure.

Table 2. Mesh convergence test for verification of elastoplastic buckling model under combined loading on unstiffened plate with rectangular perforation.

Element Length (mm)	Number of Elements	σ_u (MPa)
100	174	28.75
75	345	28.40
50	704	28.40
30	1974	28.40
25	2747	28.40

In the present study, a $\sigma_u = 28.40$ MPa was obtained with 200 sub-steps of loading. When compared to $\sigma_u = 28.76$ MPa with 1000 sub-steps of loading by Baumgardt et al. [11], the result is 1.25% lower. Despite the different reference loading sub-steps considered in each model, the ultimate stress values also confirm that the proposed model is verified for use in the elastoplastic analysis of unstiffened plates.

3.1.2. Verification of Elastoplastic Buckling Model Under Combined Loading on Stiffened Plates

The first verification was developed considering Paik and Seo [24] study, and its results from ANSYS (version 10.0), ALPS/ULSAP (version 2006.3), and DNV PULS (version 2.05) software's, through the application of longitudinal compressive loading σ_X and transverse compressive σ_Y loading in different ratios, and a constant lateral pressure P_z = 0.16 MPa to a simply supported stiffened plate with E = 208.5 GPa, σ_y =315 MPa, ν = 0.3, a = 16300 mm, b = 4300 mm, and t_p = 19 mm. The stiffeners present a T-shape, with t_s = 10 mm, h_s = 100 mm, and flange with thickness t_f = 17 mm and height h_f = 172 mm. The initial imperfections were considered as w_0 = 4.07 mm from plate, w_w = 0.5 mm for stiffeners web, and w_f = 4.2 mm for fabrication-related initial distortions. The proposed model considered $w_0 = b/2000$ = 2.15 mm (Equation (8)) from the first buckling mode. The geometry of the stiffened plate with boundary conditions of the proposed model is shown in Figure 10.

The finite element size used in the proposed model was defined according to the mesh convergence test considering the loading condition σ_X:σ_Y = 0.79:0.21, presented in Table 3.

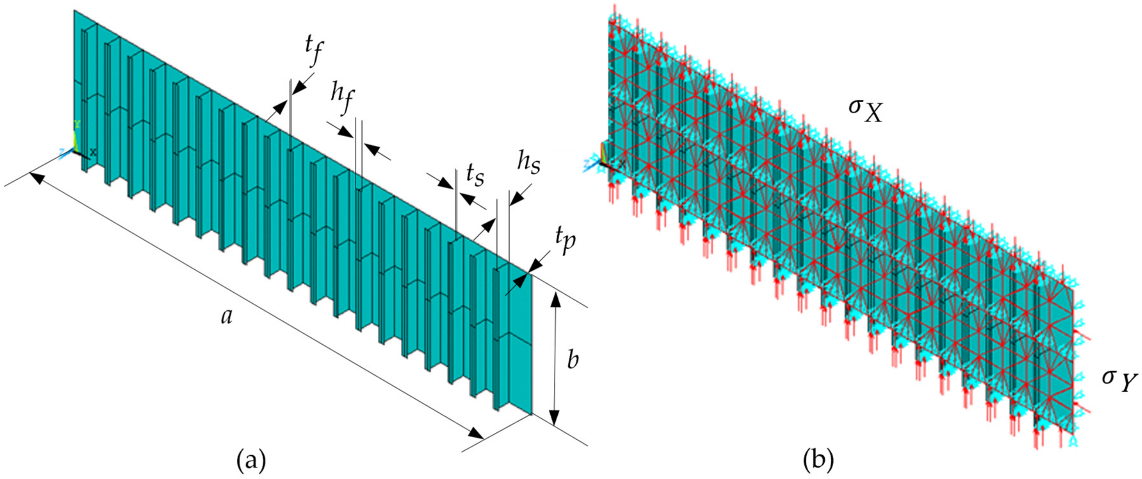

Figure 10. Stiffened plate: (**a**) geometry and (**b**) boundary conditions of the proposed model, with the blue symbols representing the displacement constraints according to the axis direction, the red arrows representing the biaxial compressive loading, and the red lines on the plate representing the applied lateral pressure.

Table 3. Mesh convergence test for verification of elastoplastic buckling model under combined loading on stiffened plates.

Element Length (mm)	Number of Elements	σ_{uX} (MPa)
600	776	236.25
500	970	236.25
250	4290	236.25

The results of σ_{uX} and σ_{uY} from the present study and from reference are shown in Table 4.

Table 4. Results of σ_{uX} and σ_{uY} obtained from the present study and from Paik and Seo [24].

σ_{uX}:σ_{uY} Ratio	Present Study		Paik and Seo [24]					
			ANSYS		ALPS/ULSAP		DNV PULS	
	σ_{uX}	σ_{uY}	σ_{uX}	σ_{uY}	σ_{uX}	σ_{uY}	σ_{uX}	σ_{uY}
0.79:0.21	236.25	62.80	223.65	59.85	199.33	53.55	245.70	66.15
0.40:0.60	76.65	114.97	66.78	100.17	62.02	93.02	73.05	109.56

For σ_{uX}:σ_{uY} = 0.79:0.21, the present study achieved σ_{uX} = 236.25 MPa and σ_{uY} = 62.80 MPa, showing differences of 5.63% and 4.93% compared to the ANSYS results, 18.52% and 17.27% compared to the ALPS/ULSAP results, and −3.85% and −5.06% compared to the DNV PULS results from Paik and Seo [24]. For the loading condition σ_{uX}:σ_{uY} = 0.40:0.60, the present study resulted in σ_{uX} = 76.65 MPa and σ_{uY} = 114.97 MPa, showing, respectively, differences of 14.78% and 14.77% compared to the ANSYS results, 23.59% and 23.60% compared to the ALPS/ULSAP results, and 4.93% and 4.94% compared to the DNV PULS results from Paik and Seo [24]. These differences in results can be attributed to the distinct boundary conditions and the different considerations for initial imperfections between the models. However, the present study demonstrated comparable values with those of Paik and Seo [24].

The second verification of elastoplastic buckling model under combined loading on stiffened plates was carried out based on the study of Beg et al. [25], which presents the

P_u through FEM model. Moreover, the σ_{cr} of this stiffened plate using different solution methodologies (EBPlate (a) and (b), FEM using ABAQUS version 6.7, and the EN1993-1-5 A.2 standard [26]) is also presented in Beg et al. [25], allowing a verification of the proposed elastic buckling model. The studied stiffened plate has material properties of E = 210 GPa, ν = 0.3, and σ_y = 355 MPa, with dimensions a = 1800 mm, b = 1800 mm, t_p = 12 mm, t_s = 10 mm, and h_s = 100 mm, being submitted to a compressive uniaxial loading, as depicted in Figure 11.

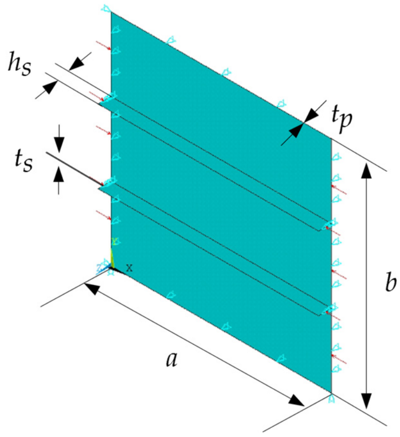

Figure 11. Modeling of plate with two longitudinal stiffeners, with the blue symbols representing the displacement constraints according to the axis direction and the red arrows representing the uniaxial compressive loading.

This computational model achieved the σ_{cr} and P_u through the mesh convergence test, shown in Table 5.

Table 5. Mesh convergence test for verification of elastic and elastoplastic models of stiffened plate.

Element Length (mm)	Number of Elements	σ_{cr} (MPa)	P_u (kN)
100	396	277.73	4524.12
75	672	277.76	4524.12
50	1512	277.79	4566.01
25	5904	277.79	4566.01

The results obtained are compared with the reference results in Table 6.

Table 6. Comparison of σ_{cr} and P_u results between the present study and the referenced literature.

Methodology	σ_{cr} (MPa)	Difference (%)	P_u (kN)	Difference (%)
Present study	277.76	-	4566.01	-
EBPlate (a)	276.00	0.64	-	-
EBPlate (b)	289.00	−3.89	-	-
ABAQUS	268.00	3.64	4424.00	3.21
EN1993-1-5 A.2 [26]	290.00	−4.22	-	-

The present study obtained σ_{cr} = 277.79 N/mm^2, showing a small difference when compared to other methods. The maximum difference was 4.22%, which was observed when compared to the EN1993-1-5 A.2 methodology, although with a lower value, providing safety. The smallest difference was obtained in relation to the EBPlate (a) method, with a difference of 0.64% higher. Regarding the finite element method, the difference between the result obtained in this study and the reference using ABAQUS (version 6.7) was 3.64% higher. According to the ultimate strength, the present study results in P_u = 4566.01 kN, 3.11% higher than P_u = 4424.00 kN obtained from FEM by Beg et al. [25]. Overall, the results demonstrate good consistency across the different approaches.

3.1.3. Validation of Elastoplastic Buckling Model Under Combined Loading on Stiffened Plate

The validation was performed by comparing the P_u obtained by the present study with the P_u obtained experimentally by Kumar et al. [26]. The authors applied uniaxial compressive loading and lateral pressure P_z = 0.06 MPa to a stiffened panel, illustrated in Figure 12, having a = 1160 mm, b = 960 mm, t_p = 4 mm, E = 180 GPa, ν = 0.3, and σ_{yp} = 218 MPa. The panel has four longitudinal stiffeners located with a_1 = 100 mm from the sides and spaced c_2 = 320 mm apart, as well as four transverse stiffeners spaced by b_1 = 60 mm from the ends and c_1 = 280 mm between them. The stiffeners have t_s = 5 mm, h_s = 50 mm, E = 180 GPa, ν = 0.3, and σ_{ys} = 300 MPa.

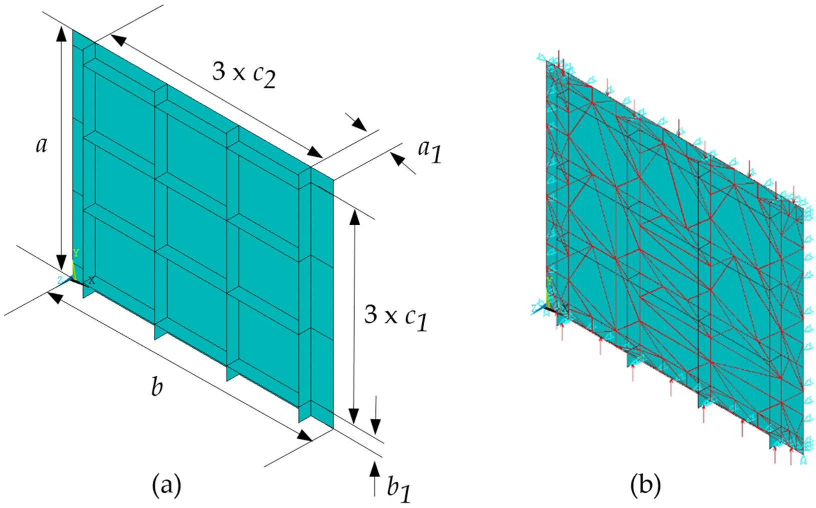

Figure 12. Stiffened plate considered in validation: (**a**) dimensions and (**b**) loading and boundary conditions, with the blue symbols representing the displacement constraints according to the axis direction, the red arrows representing the biaxial compressive loading, and the red lines on the plate representing the applied lateral pressure.

For the proposed model, the σ_u was obtained with the mesh convergence test. The obtained values of σ_u are presented in Table 7.

Table 7. Mesh convergence test for validation of σ_u under combined loading.

Element Length (mm)	Number of Elements	σ_u (MPa)
75	382	140.32
50	894	123.55
35	1472	123.25
20	3936	122.90

This model results in σ_u = 122.90 MPa, with an error of 0.39% compared to the experimental result of σ_u = 123.38 MPa obtained by Kumar et al. [26]. The displacements and von Mises stress distributions are shown in Figure 13.

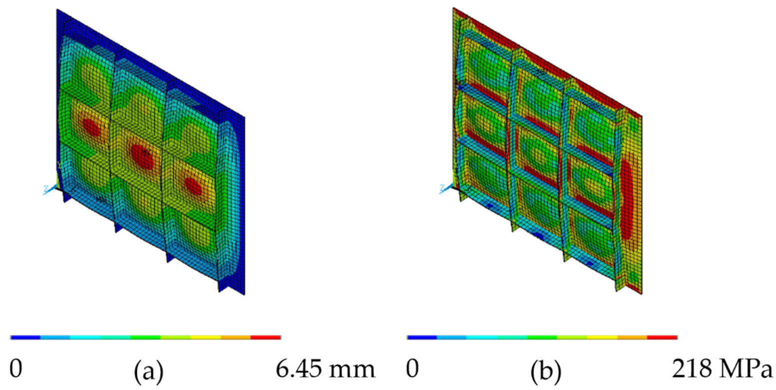

Figure 13. Validation of elastoplastic buckling of stiffened plates due combined loading: (**a**) U_z and (**b**) von Mises stress distribution.

The σ_u obtained for the stiffened panel under combined loading aligns well with the experimental result of Kumar et al. [26]. The transverse stiffeners presented less stress concentration than longitudinal, meaning that the stiffeners in the loading direction are responsible for supporting majority stress, corroborating with Lima et al.'s [13] conclusions about that. Therefore, both quantitatively and qualitatively, the computational model was duly validated.

3.2. Case Study

3.2.1. Mesh Convergence Test

The mesh convergence test was conducted to standardize the mesh element size based on the P(2;2) plate configuration with h_s/t_s = 1.02, under P_z = 0.16 MPa and biaxial compression, which were divided into 100 sub-steps. The results of σ_u are shown in Table 8.

From Table 8, one can infer that the mesh convergence test obtained the same σ_u value for element size with 25 mm, 20 mm, and 10 mm. Considering the element size with 25 mm results in a computational effort reduction by 27% and 84% being achieved, respectively. Moreover, the difference in the von Mises stress distribution is depicted in Figure 14.

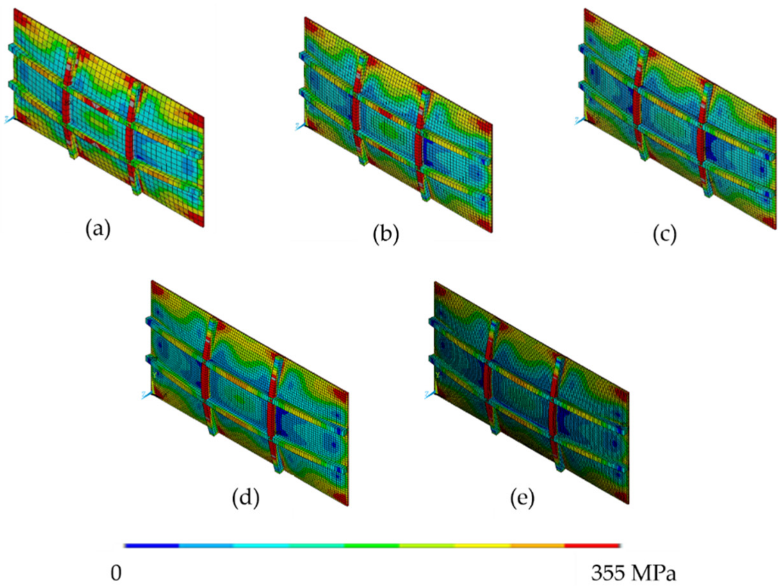

Figure 14. The von Mises stress distribution of plates with finite element size of: (**a**) 50 mm, (**b**) 30 mm, (**c**) 25 mm, (**d**) 20 mm, and (**e**) 10 mm.

Table 8. Mesh convergence test for plate configuration P(2;2) with $h_s = 45.82$ mm and $t_s = 45$ mm.

Element Length (mm)	Number of Elements	Processing Time (s)	σ_u (MPa)
50	1134	82	101.17
30	3114	112	99.40
25	4140	158	97.62
20	6426	216	97.62
10	24,744	975	97.62

Although in some cases the difference in mesh element size does not impact the σ_u, there is a difference in the obtained stress distribution. Therefore, based on Table 8 and Figure 14, the mesh element size adopted for all case studies is 25 mm.

3.2.2. Sub-Steps Convergence Test

The sub-steps convergence test was conducted to standardize the number of sub-steps that the reference loads will be divided and applied. This study is also based on the P(2;2) plate configuration with $h_s/t_s = 1.02$, under $P_z = 0.16$ MPa and biaxial compression, with a finite element size of 25 mm. The results of σ_u are shown in Table 9.

Table 9. Number of sub-steps test for plate configuration P(2;2) with $h_s = 45.82$ mm and $t_s = 45$ mm.

Number of Sub-Steps	Maximum Number of Sub-Steps	Minimum Number of Sub-Steps	Processing Time (s)	σ_u (MPa)
100	200	50	168	97.62
200	400	100	212	98.51
300	600	150	385	98.51
400	800	200	440	98.51

The results in Table 9 indicate that dividing the reference load into 100 sub-steps versus 200, 300, and 400 resulted in only a −0.9% difference in σ_u, but reduced computational effort by 21%, 56%, and 62, respectively. In addition, the von Mises stress distribution for each case of Table 9 is presented in Figure 15.

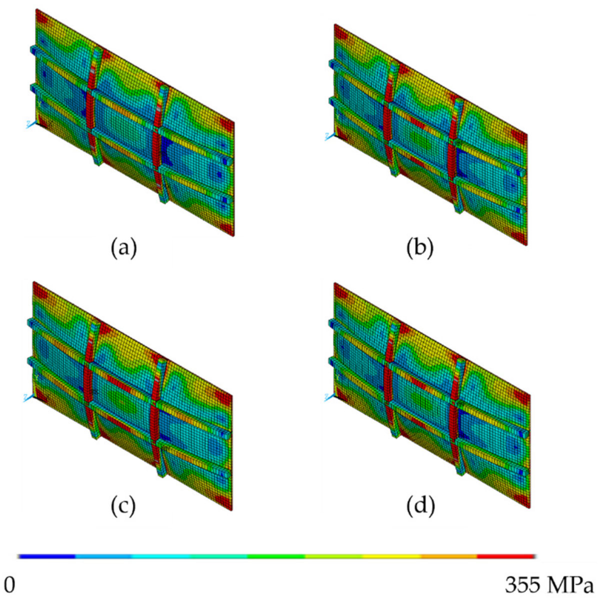

Figure 15. The von Mises stress distribution of plates with number of sub-steps: (**a**) 100, (**b**) 200, (**c**) 300, and (**d**) 400.

From Figure 15, the stress values and distributions showed a slight discrepancy when considering the different sub-steps. Therefore, to reduce the computational effort, all case study simulations were performed with 100 sub-steps of loading, which can achieve a maximum of 200 and a minimum of 50 sub-steps according to problem convergence.

3.3. Geometric Evaluation

This section presents and discusses the results of the analysis with the constructal design method and exhaustive search technique. To do so, the influence of P_z direction application and degrees of freedom variation on the ultimate biaxial buckling stress of stiffened plates was investigated, allowing to identify the maximized stress and their respective optimized geometric configurations.

3.3.1. Reference Plate

The reference plate was defined as an unstiffened plate with dimensions a = 2000 mm, b = 1000 mm, and t = 20 mm; made of AH-36 steel, with material properties E = 210 GPa, ν = 0.3, and σ_y= 355 MPa; and subjected to a lateral loading $P_z = 0.16$ MPa. The application of P_z resulted in an out-of-plane maximum displacement of $U_z = 10.40$ mm located at the center of the plate (Figure 16a). Thereafter, with the subsequent application of the biaxial compressive loading, this displacement achieved $U_z = 40.19$ mm (Figure 16b), resulting in $\sigma_{uR} = 44.37$ MPa (Figure 16c).

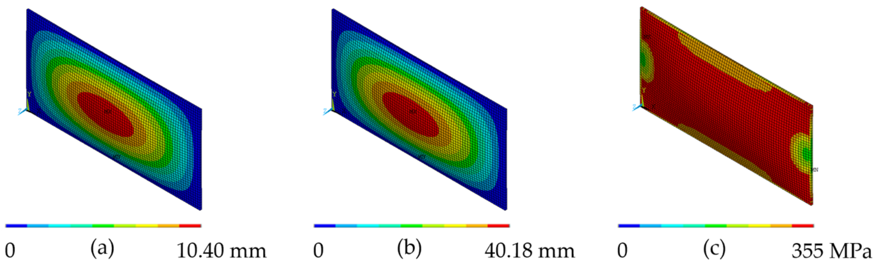

Figure 16. Unstiffened plate with application of $P_z = 0.16$ MPa: (**a**) U_z due lateral pressure, (**b**) U_z due application of lateral pressure and biaxial compression, and (**c**) von Mises stress distribution due application of lateral pressure and biaxial compression.

3.3.2. Influence of P_z and h_s/t_s over σ_{uN}

Two distinct behaviors from the influence of P_z and h_s/t_s over σ_{uN} were identified in this study: in stiffened plates having $N_{ls} < 4$ (represented in Figure 17 by stiffened plates N_{ls} = 2) and those with $N_{ls} \geq 4$ (represented by stiffened plates with N_{ls} = 4, which will be presented and discussed later).

In stiffened plates with $N_{ls} < 4$, from Figure 17, it can be noted that the application of positive lateral pressure reduced the σ_{uN}, while negative lateral pressure increased σ_{uN}. For positive pressure, lower values of h_s/t_s resulted in a severe reduction in σ_{uN}. This can be explained by the displacement resulting from the application of positive lateral pressure and subsequent biaxial loading, as illustrated in Figure 18.

In plate configurations with $N_{ls} < 4$, one can observe in Figure 18 that lower values of h_s/t_s resulted directly in a global displacements distribution (Figure 18a), and the subsequent application of the biaxial loading maintained this mechanical behavior (Figure 18b), increasing the out-of-plane displacements and leading to a quick structural collapse. On the other hand, higher values of h_s/t_s resulted in local displacements distribution due to the application of lateral pressure (Figure 18c). With the subsequent application of biaxial loading, the displacements just evolved until the local collapse of the stiffened plate (Figure 18d). So, in the graphics on Figure 17, at the values of h_s/t_s the σ_{uN} increased, and the stiffened plates geometry results into local displacements until collapse.

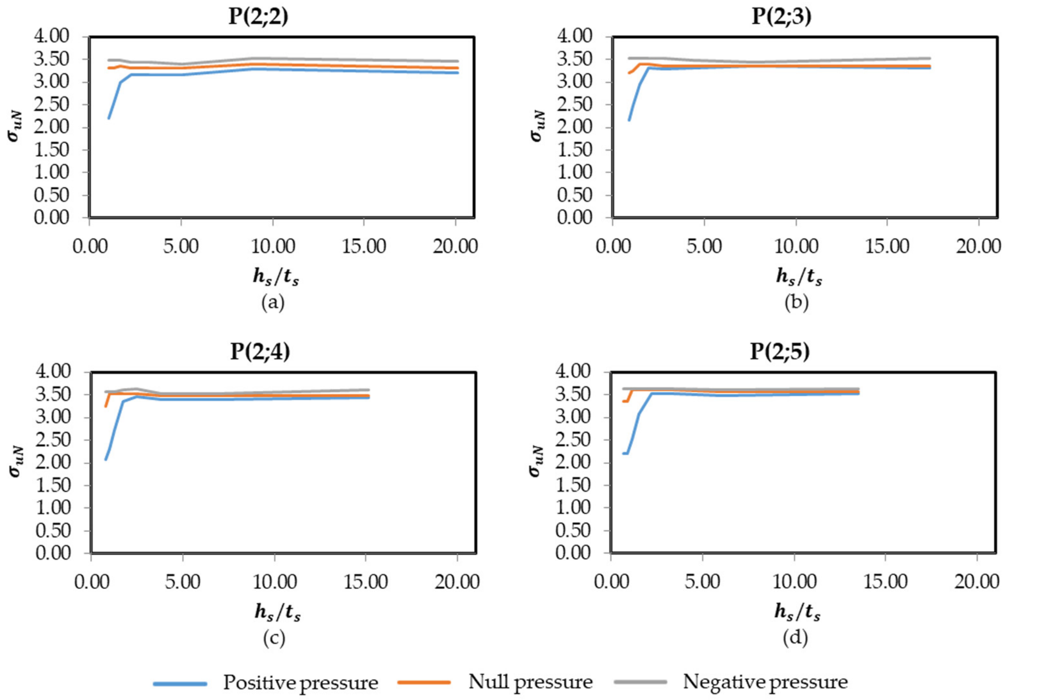

Figure 17. Influence of h_s/t_s and lateral pressure P_z on σ_{uN} in plates with $N_{ls} < 4$: (**a**) P(2;2), (**b**) P(2;3), (**c**) P(2;4), and (**d**) P(2;5).

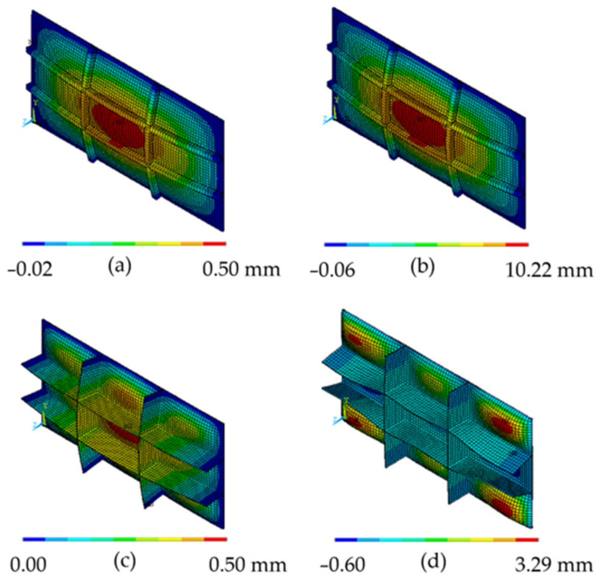

Figure 18. Influence of h_s/t_s, positive lateral pressure, and subsequent biaxial compressive loading on displacements of plates with N_{ls} < 4: (**a**) h_s/t_s = 1.02 and lateral pressure, (**b**) h_s/t_s = 1.02, lateral pressure, and biaxial loading, (**c**) h_s/t_s = 20.13 and lateral pressure, and (**d**) h_s/t_s = 20.13, lateral pressure, and biaxial loading.

Also, for plates configurations with $N_{ls} < 4$, the negative pressure improved σ_{uN}. It can be explained by the displacement resulting from negative lateral pressure and subsequent biaxial loading, shown in Figure 19, in which lower values of h_s/t_s resulted in global displacements distribution due to the application of lateral pressure (Figure 19a), and subsequent application of biaxial loading overcame these displacements, resulting in local displacements until collapse (Figure 19b). Higher values of h_s/t_s resulted in local displacements due to the application of lateral pressure (Figure 19c), and the subsequent application of biaxial loading also overcame these displacements until the local collapse (Figure 19d). From this reason, there is no significant variation on σ_{uN} in the graphics in

Figure 17, indicating that all h_s/t_s values led to local displacements due to the application of biaxial compressive loading until local collapse.

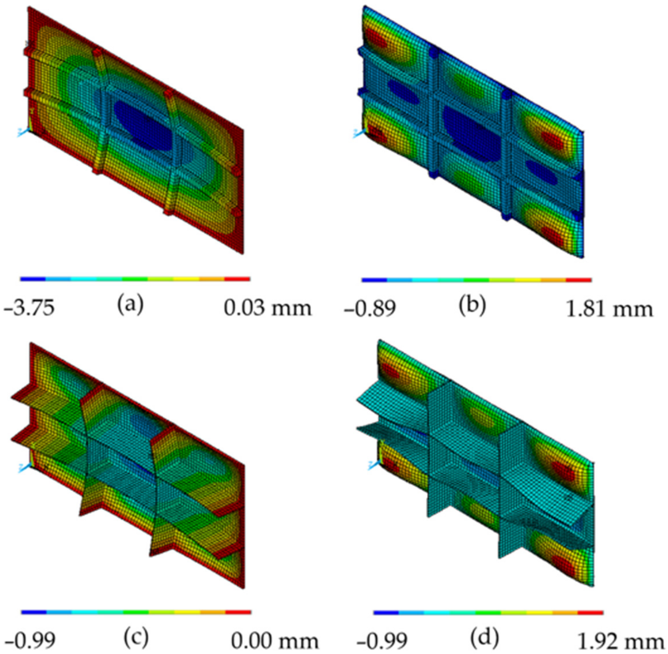

Figure 19. Influence of h_s/t_s, negative lateral pressure, and subsequent biaxial compressive loading on displacements of plates with $N_{ls} < 4$: (**a**) h_s/t_s = 1.02 and lateral pressure, (**b**) h_s/t_s = 1.02, lateral pressure, and biaxial loading, (**c**) h_s/t_s = 20.13 and lateral pressure, and (**d**) h_s/t_s = 20.13, lateral pressure, and biaxial loading.

In turn, the results for the stiffened plates with $N_{ls} \geq 4$ is presented in Figure 20, represented by the cases with $N_{ls} = 4$.

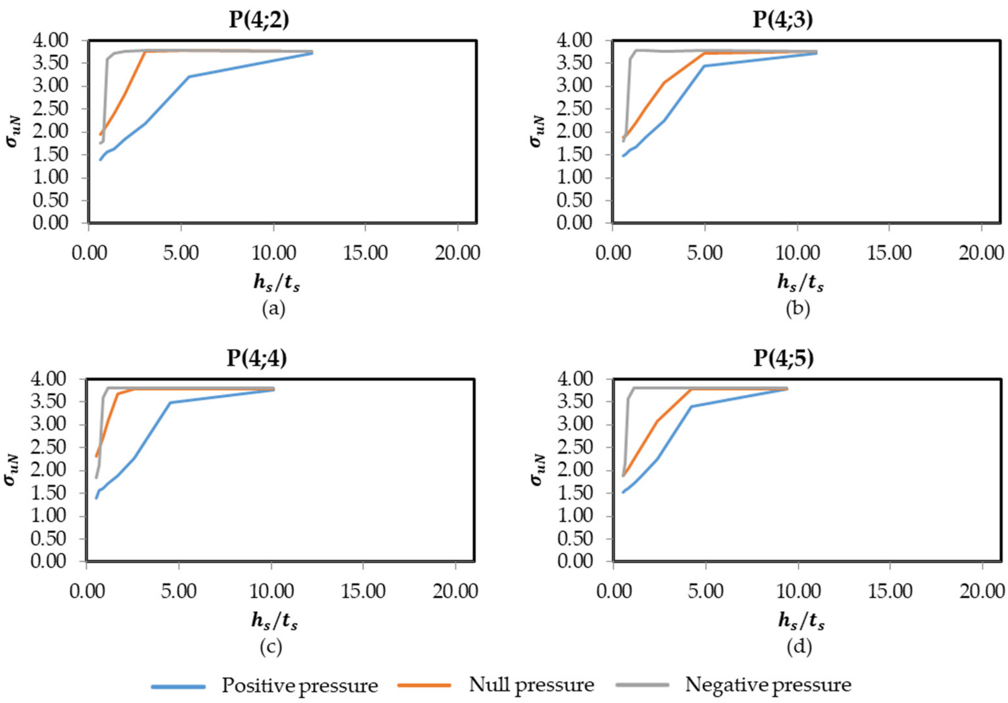

Figure 20. Influence of h_s/t_s and lateral pressure on σ_{uN} in plates with $N_{ls} \geq 4$: (**a**) P(4;2), (**b**) P(4;3), (**c**) P(4;4), and (**d**) P(4;5).

It is interesting to emphasize that due to the conservation of the total volume of the stiffened plates (Equation (15)), the increasing number of stiffeners requires reducing the maximum and minimum available h_s/t_s values to respect this premise, consequently propitiating global displacements distributions.

In Figure 20, for lower values of h_s/t_s, the application of positive lateral pressure leads to global displacements distributions, which evolve into global collapse due to compressive biaxial loading, resulting in low values of σ_{uN} for these geometric configurations. While for higher values of h_s/t_s, the lateral pressure induces global displacements distributions that evolve into local displacements collapse, resulting in the best σ_{uN} values for these plate configurations.

Figure 20 also indicates that the negative lateral pressure increased or decreased σ_{uN} according to h_s/t_s values. This fact can be explained by the resulting displacements due to negative lateral pressure application and subsequent biaxial loading, as illustrated in Figure 21.

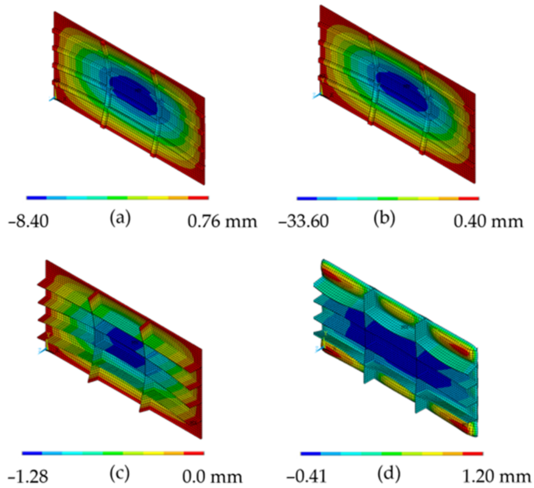

Figure 21. Influence of h_s/t_s, negative lateral pressure, and subsequent biaxial compressive loading on displacements of plates with $N_{ls} \geq 4$: (**a**) h_s/t_s = 0.61 and negative lateral pressure, (**b**) h_s/t_s = 0.61, negative lateral pressure, and biaxial loading, (**c**) h_s/t_s = 12.10 and lateral pressure, and (**d**) h_s/t_s = 12.10, negative lateral pressure, and biaxial loading.

In Figure 21, one can infer that lower values of h_s/t_s led to negative global displacements distributions due to the application of negative P_z (Figure 21a), and the subsequent application of biaxial loading contributed to these negative displacements and consequently considerably reduced σ_{uN}, causing the structural collapse (Figure 21b). Whilst higher values of h_s/t_s resulted in negative global displacements distributions due to negative P_z application (Figure 21c), and the subsequent application of biaxial compressive loading resulted in positive displacements (Figure 21d), overcame negative displacements and consequently improved σ_{uN}, collapsing with local displacements (Figure 21b) and achieving better values of σ_{uN}. With this, for negative pressure application (Figure 20), at the h_s/t_s as σ_{uN} presented lower values, the stiffened plate displacements maintained global displacements distributions from negative lateral pressure to biaxial loading until collapse, and the increase of h_s/t_s resulted in higher values of σ_{uN}, indicating that the biaxial loading overcame the global displacements into local displacements until collapse.

It could be stated that lower values of N_{ls} allow for higher values of h_s/t_s, but in contrast, this results in an increased spacing S_{ls} between them, leading to local displacements on the stiffened plate, which tends to improve σ_{uN}. On the other hand, higher values of N_{ls} reduce the spacing S_{ls}, but the necessary reduction in h_s/t_s to maintain the constant volume constraint makes the stiffened plate more susceptible to global displacement distribution, tending to reduce σ_{uN}.

3.3.3. Highest Values of h_s/t_s, N_{ls}, and N_{ts} over σ_{uN}

The highest value of σ_{uN} was 3.84, reached from the P(5;4) with h_s/t_s = 8.74 and from the P(5;5) with h_s/t_s = 8.14, and the P(5;4) selected as better due its lower displacements. The lowest value of σ_{uN} was 1.22 achieved by P(3;5) with h_s/t_s = 0.57. These highest and lowest values represent an increase on σ_{uR} of 284% and 22%, respectively. The displacement and von Mises stress distributions for both cases are depicted in Figure 22.

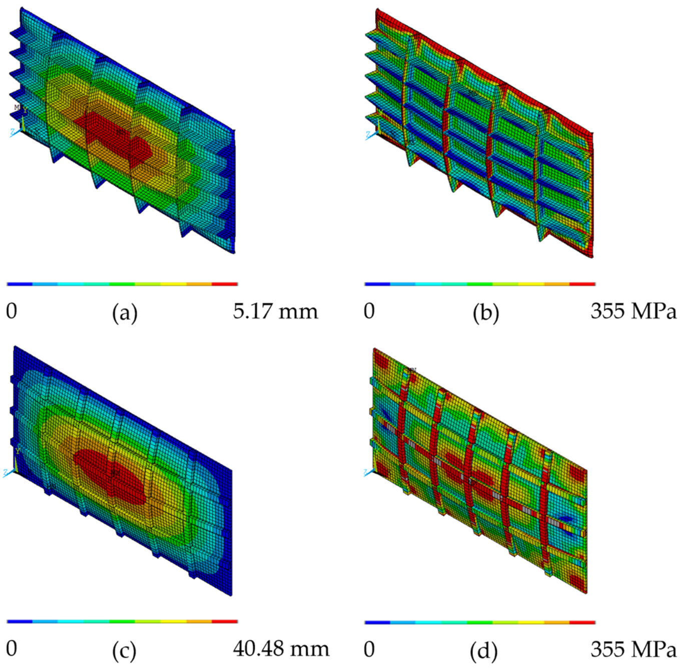

Figure 22. Best and worst plate configurations displacements and von Mises stress distribution: (**a**) P(5;4) displacements, (**b**) P(5;4) stress distribution, (**c**) P(3;5) displacements, and (**d**) P(3;5) stress distribution.

The best configuration collapsed with local displacements (Figure 22a), while the worst configuration collapsed with global displacements (Figure 22c). In comparison with their von Mises stress distribution, it noted that the stiffened plate which presented the best stress distribution resulted in the highest σ_{uN} (Figure 22b). Conversely, the stiffened plate with the worst stress distribution (Figure 22d) displayed the lowest value of σ_{uN}, in accordance with the constructal law.

3.3.4. Influence of N_{ls} and N_{ts} over Once Optimized $(h_s/t_s)_o$ and Once Maximized $(\sigma_{uN})_m$

From the results of σ_{uN} for each h_s/t_s value in each plate configuration, the $(\sigma_{uN})_m$ and their respective $(h_s/t_s)_o$ were obtained, as described in Table 10.

Based on the results of Table 10, the highest value of $(\sigma_{uN})_m$ was 3.84, achieved by P(5;4) with $(h_s/t_s)_o$ = 8.70, while the lowest value of $(\sigma_{uN})_m$ was 3.28, reached from the P(2;2) with $(h_s/t_s)_o$ = 8.98. These highest and lowest values represent an increase on σ_{uR} of 284% and 228%, respectively. The displacements and stress distributions are shown in Figure 23, with both P(5;4) and P(2;2) collapsing with local displacements. In comparison with their von Mises stress distribution, it can be noted that the stiffened plate which presented the best stress distribution between plate and stiffeners resulted in the highest $(\sigma_{uN})_m$ (Figure 23b), while the stiffened plate that presented the worst stress distribution (Figure 23d) resulted in the lowest $(\sigma_{uN})_m$, also respecting the constructal law.

Table 10. $(\sigma_{uN})_m$ and $(h_s/t_s)_o$ for plate configurations.

Plate Configuration	N_{ls}	N_{ts}	$(h_s/t_s)_o$	$(\sigma_{uN})_m$
P(2;2)	2	2	8.98	3.28
P(2;3)	2	3	7.72	3.36
P(2;4)	2	4	2.46	3.46
P(2;5)	2	5	13.48	3.52
P(3;2)	3	2	15.11	3.56
P(3;3)	3	3	13.47	3.60
P(3;4)	3	4	12.15	3.64
P(3;5)	3	5	11.06	3.68
P(4;2)	4	2	12.10	3.72
P(4;3)	4	3	11.03	3.72
P(4;4)	4	4	10.14	3.76
P(4;5)	4	5	9.38	3.78
P(5;2)	5	2	10.08	3.78
P(5;3)	5	3	9.34	3.80
P(5;4)	5	4	8.70	3.84
P(5;5)	5	5	8.14	3.84

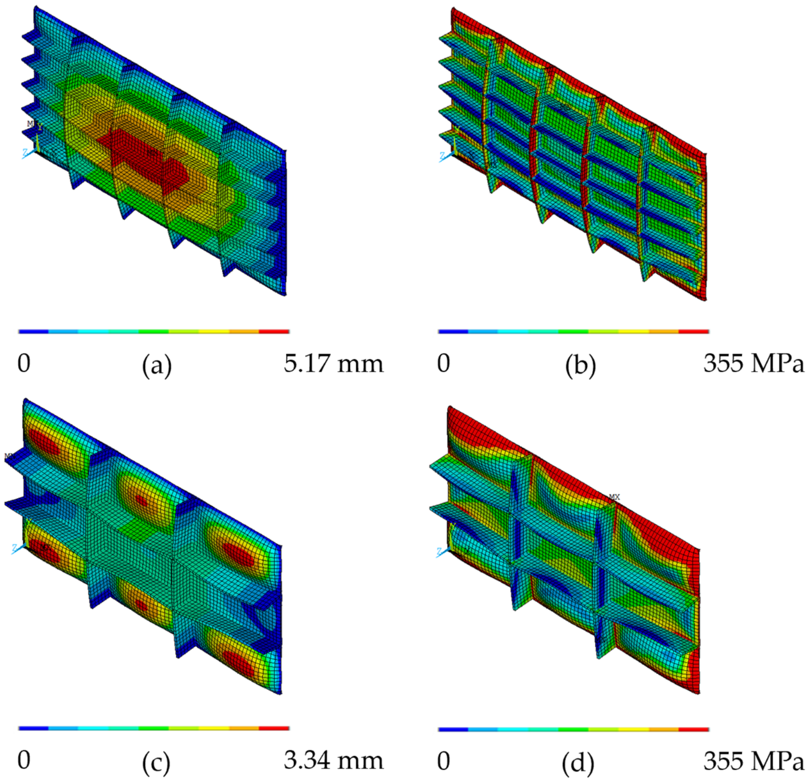

Figure 23. Displacements and von Mises stress distribution of best and worst plate configurations on $(\sigma_{uN})_m$: (**a**) P(5;4) displacements, (**b**) P(5;4) stress distribution, (**c**) P(2;2) displacements, and (**d**) P(2;2) stress distribution.

The influence of N_{ls}, N_{ts}, and $(h_s/t_s)_o$ on $(\sigma_{uN})_m$ from Table 7 was plotted in Figure 24. The increase in N_{ls} and N_{ts} improved $(\sigma_{uN})_m$ and, in general, the $(\sigma_{uN})_m$ was obtained by higher values of $(h_s/t_s)_o$ from most respective plate configurations, except for plates with P(2;2), P(2;3), and P(2;4). To understand this aspect, the plate configuration P(2;4) served as a model to investigate this behavior through comparison of the resulting displacements and von Mises stress distributions, depicted in Figures 25 and 26 (in which the red color on stiffened plate images represents the maximum values and the blue color represents the minimum values).

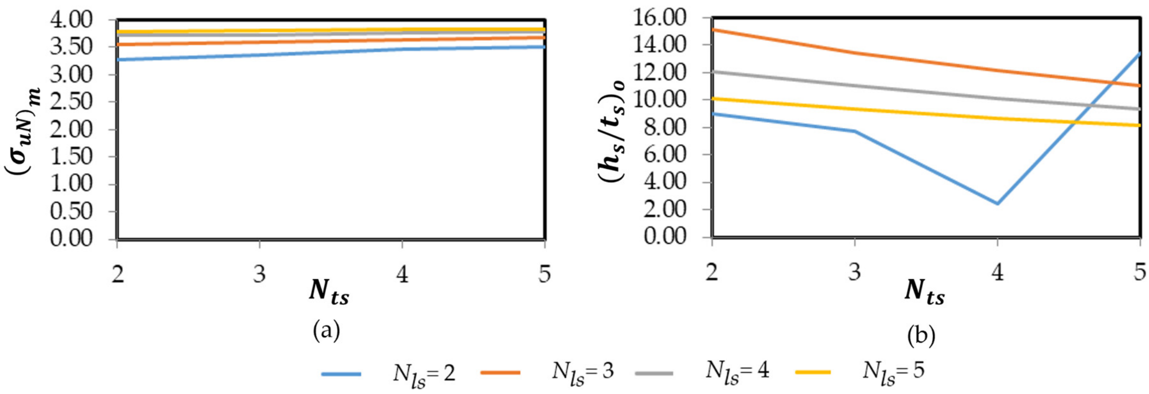

Figure 24. Influence of N_{ls} and N_{ts} on: (**a**) $(\sigma_{uN})_m$ and (**b**) $(h_s/t_s)_o$.

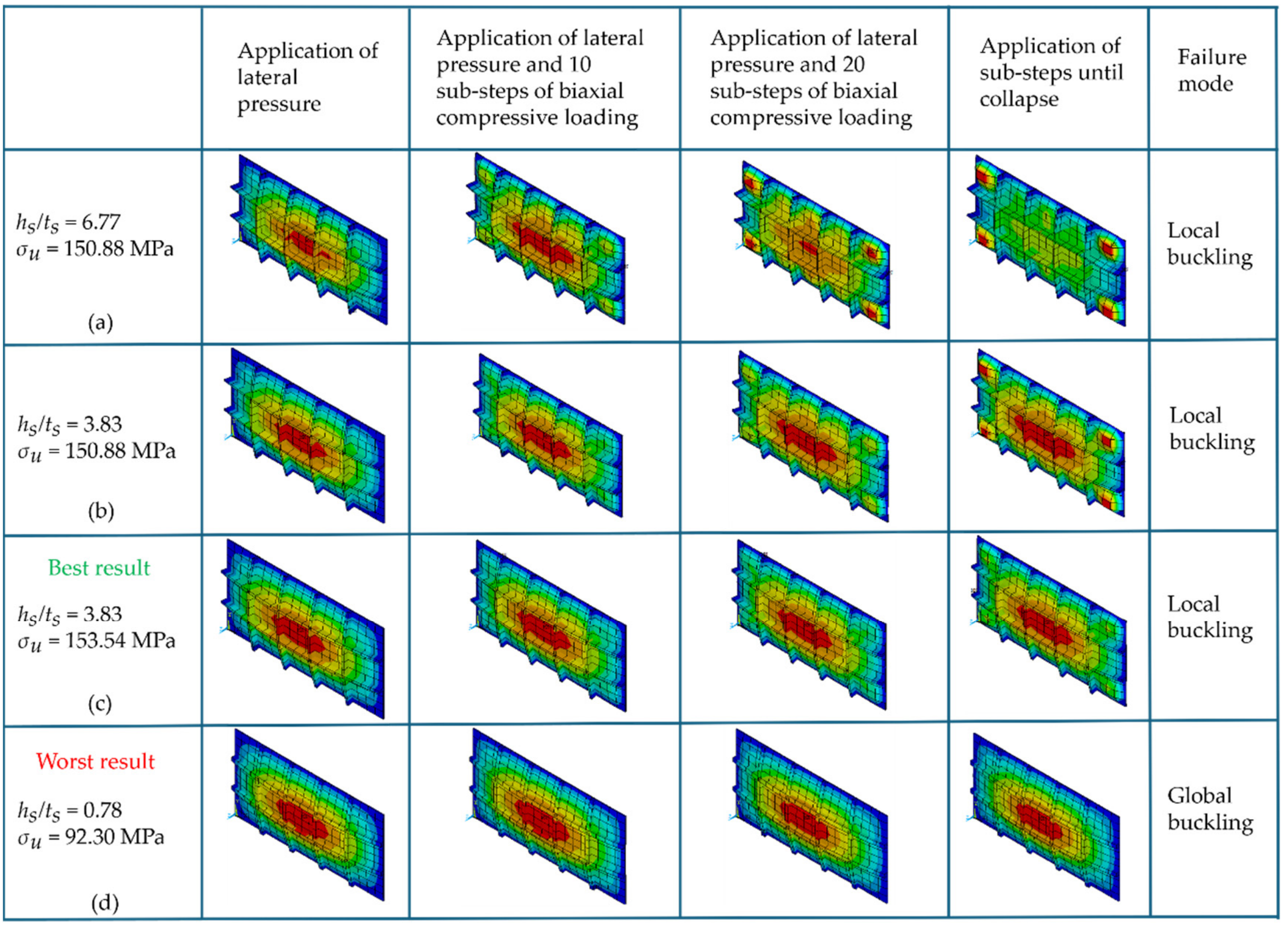

Figure 25. Results of the application of lateral pressure and subsequent compressive biaxial loading on displacements of P(2;4) with different values of h_s/t_s: (**a**) h_s/t_s = 6.77, (**b**) h_s/t_s = 3.83, (**c**) h_s/t_s = 2.46, and (**d**) h_s/t_s = 0.78.

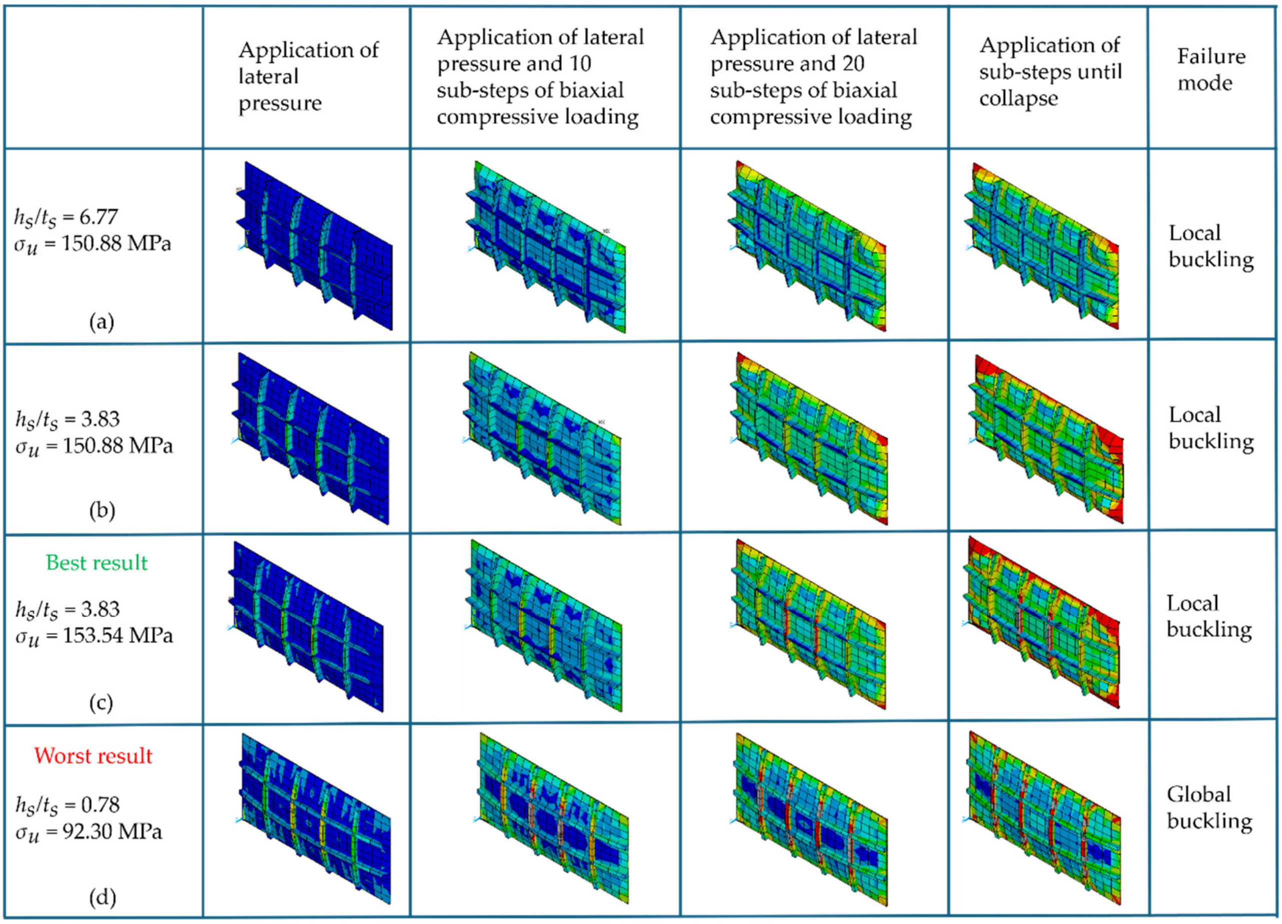

Figure 26. Results of the application of lateral pressure and subsequent biaxial compressive loading on von Mises stress of P(2;4) with different values of h_s/t_s: (**a**) h_s/t_s = 6.77, (**b**) h_s/t_s = 3.83, (**c**) h_s/t_s = 2.46, and (**d**) h_s/t_s = 0.78.

Several key findings can be drawn from the behavior of the stiffened plate configurations P(2;2), P(2;3), and P(2;4), as seen in Figures 25 and 26. The ratio h_s/t_s significantly influenced σ_{uN}, with the potential to either improve or reduce the ultimate strength of the stiffened plate. For the highest value h_s/t_s = 6.77 (Figure 25a), the moment of inertia of the stiffeners was so high that it limited their U_z displacements, acting close to dividing the plate into smaller sections. Due to the low number of longitudinal stiffeners, the spacing S_{ls} between them was significant, allowing the plate to displace into areas less influenced by the stiffeners, such as the upper and lower corners. Hence, when lateral pressure and biaxial compressive loading were applied, high displacements occurred at the plate corners, leading to local displacements and collapse. The stress distribution in this case (Figure 26a) showed a poor distribution, with a high concentration of stress only in the plate, ultimately resulting in local collapse.

When h_s/t_s was reduced to 3.83, the moment of inertia of stiffeners decreased, allowing the stiffeners to displace in U_z (Figure 25b). This behavior improved the distribution of displacements across the plate and the stiffeners, including at the upper and lower corners and at the center of the stiffened plate. In addition, σ_{uN} was not increased with the reduction of h_s/t_s from 6.77 to 3.83, but the geometric configuration resulted in a reduction in maximum local displacements of the plate that also led to local collapse. The stress distribution (Figure 26b) also improved with the reduction of h_s/t_s, with a larger area now concentrating the stress more evenly across the plate.

Further reduction of h_s/t_s (Figure 25c) significantly improved the U_z displacement, leading to better displacement distribution between the plate and stiffeners. While the plate still experienced local displacements at the upper and lower corners without failure, local displacements at the center ultimately led to local collapse. The more balanced displacement distribution enhanced the achievement of $(\sigma_{uN})_m$ and $(h_s/t_s)_o$ for this configuration. Stress distribution (Figure 26c) also improved, with stress concentration previously limited to the plate now also distributed across the transverse stiffeners. This behavior resulted in the plate and stiffeners working together as a cohesive system, achieving the maximum value $(\sigma_{uN})_m$ for this case.

Finally, reducing h_s/t_s to the lowest value of 0.78 (Figure 25d) significantly reduced the moment of inertia of the stiffeners, improving U_z in these components and causing them to exhibit the highest displacements. The stiffeners displaced more easily along with the plate, offering minimal resistance to out-of-plane displacements. This behavior resulted in the global displacement distribution of the system, occurring early during lateral pressure application, with displacement continuing as biaxial compression progressed, ultimately leading to global collapse. In contrast to previous configurations, when h_s/t_s was significantly reduced (Figure 26d), the geometry showed the worst stress distribution and σ_{uN}. The transverse stiffeners exhibited a concentration of stress immediately after applying lateral pressure, causing global collapse before any significant stress was distributed across the plate.

3.3.5. Influence of N_{ls}, $(N_{ts})_o$, and $(h_s/t_s)_{oo}$ over $(\sigma_{uN})_{mm}$

From the results of N_{ts}, $(h_s/t_s)_o$, and $(\sigma_{uN})_m$, the once optimized $(N_{ts})_o$, the twice maximized normalized ultimate strength $(\sigma_{uN})_{mm}$, and their respective twice optimized height-to-thickness ratio $(h_s/t_s)_{oo}$ were obtained, as can be viewed in Table 11.

Table 11. Results of $(N_{ts})_o$, $(h_s/t_s)_{oo}$, and $(\sigma_{uN})_{mm}$ for N_{ls}.

Plate Configuration	N_{ls}	$(N_{ts})_o$	$(h_s/t_s)_{oo}$	$(\sigma_{uN})_{mm}$
P(2;5)	2	5	13.48	3.52
P(3;5)	3	5	11.06	3.68
P(4;5)	4	5	9.38	3.78
P(5;4)	5	4	8.70	3.84

The highest value of $(\sigma_{uN})_{mm}$ was 3.84, achieved by P(5;4) with $(h_s/t_s)_{oo}$ = 8.70, and the lowest value of $(\sigma_{uN})_{mm}$ was 3.52, reached from the P(2;5) with $(h_s/t_s)_{oo}$ = 13.48. These highest and lowest values represent an increase on σ_{uR} of 284% and 252%, respectively. The displacements and stress distribution are illustrated in Figure 27.

As previously discussed, the highest value was obtained from P(5;4), which exhibited a geometric configuration that enabled the best distribution of displacements (Figure 27a) and stresses (Figure 27b) between the plate and stiffeners. In contrast, for P(2;5), the lowest value of $(\sigma_{uN})_{mm}$ resulted from poor displacement (Figure 27c) and stress distribution (Figure 27d), caused by the very high value of $(h_s/t_s)_{oo}$. This behavior led to the highest moment of inertia, which restricted U_z displacements of stiffeners and acted close to dividing the plate into smaller sections. Additionally, the low number of N_{ls} increased the spacing S_{ls} between them. As a result, displacements and stresses became concentrated in areas with less contact with the stiffeners, specifically the upper and lower corners of the plate, with no significant stresses in the stiffeners, leading to a local collapse.

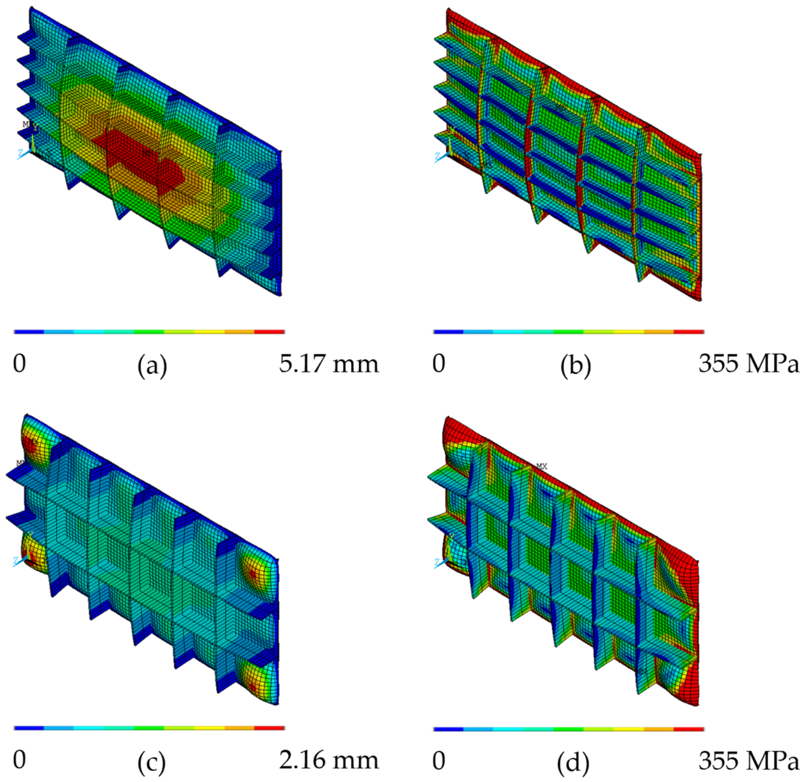

Figure 27. Displacements and von Mises stress distribution of best and worst plate configurations on $(\sigma_{uN})_{mm}$: (**a**) P(5;4) displacements, (**b**) P(5;4) stress distribution, (**c**) P(2;5) displacements, and (**d**) P(2;5) stress distribution.

The influence of N_{ls}, $(N_{ts})_o$, and $(h_s/t_s)_{oo}$, over $(\sigma_{uN})_{mm}$ are graphically shown in Figure 28.

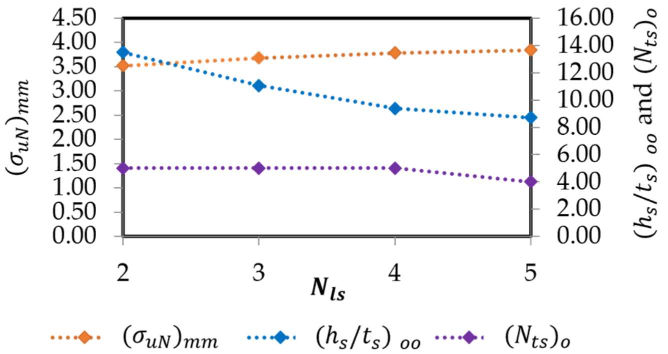

Figure 28. Influence of N_{ls} over $(N_{ts})_o$, $(h_s/t_s)_{oo}$, and $(\sigma_{uN})_{mm}$.

From Figure 28, the plate configurations that had $(\sigma_{uN})_{mm}$ presented in majority, the highest value of $(N_{ts})_o$ for each N_{ls}. Only the plate P(5;4) presented less value of $(N_{ts})_o$, but as discussed previously, both P(5;5) and P(5;4) presented the same value of $(\sigma_{uN})_m$, however P(5;4) presented less value of U_z, being maximized. Finally, as the increase of N_{ls}, the values of $(h_s/t_s)_{oo}$ that resulted in $(\sigma_{uN})_{mm}$ were the highest from each plate configuration.

4. Conclusions

Through the verification and validation of a numerical model capable of performing elastoplastic analyses of unstiffened and stiffened plates under combined loading, consisting of biaxial compression and lateral pressure, it was possible to apply the constructal design and exhaustive search to understand insights into the elastoplastic buckling behavior. The computational model was verified and validated, respectively, achieving a difference of 3.64% compared to another numerical model and a maximum error of 1.57% compared to the experimental reference. Thereafter, by converting part of the reference plate volume into stiffener volume, all proposed geometric configurations increased σ_{uN}. The geometry that showed the maximized normalized ultimate buckling stress was P(5;4), with $(\sigma_{uN})_{mmm}$= 3.84, $(h_s/t_s)_{ooo}$= 8.70, $(N_{ts})_{oo}$ =4, and $(N_{ls})_o = 5$, representing a 284% improvement compared to σ_{uR} of the unstiffened plated adopted as the reference. In addition, the optimized stiffened plate geometry was 262% superior to the worst stiffened plate geometry P(5;3), with σ_{uN} = 1.22 and h_s/t_s= 0.57.

Several relevant conclusions were drawn from this work. The mesh element size and the number of sub-steps in the load application slightly affect the ultimate strength, displacements, and stress distribution of the plates. The application of lateral pressure opposite to the displacement due to biaxial compression can increase buckling resistance by helping to prevent displacements or decrease buckling resistance adding displacements. Converting part of the plate volume into stiffeners can increase the ultimate buckling strength, but it is necessary to determine a better geometric configuration to achieve the best results. The N_{ls}, N_{ts}, and h_s/t_s ratio directly affects the displacements caused by lateral pressure and biaxial compression. Very high h_s/t_s values tend to improve the moment of inertia, prevent out-of-plane displacement of the stiffeners, concentrate stresses on the plate, and favor the occurrence of local plate collapse. Conversely, very low h_s/t_s values tend to cause the stiffeners to displace out of the plane, resulting in the global collapse of the plate and stiffeners. Therefore, the choice of the N_{ls} and N_{ts}, as well as their respective h_s/t_s, should be made to increase the stiffness of the plate–stiffener system, ensuring that both components work together. This behavior will improve the displacement and stress distribution between the plate and stiffeners, leading to higher plate ultimate strength and reduced displacements.

For future work, it is suggested to apply the developed methodology to investigate the mechanical behavior of various stiffener types, explore different plate a/b aspect ratios, and analyze the effects of cyclic loading, welding, and corrosion, together with combined loadings and how the design can improve the ultimate buckling stress in these conditions.

Supplementary Materials: The following supporting information can be downloaded at: https://www.mdpi.com/article/10.3390/app15063354/s1, Table S1: Constructal design application; Table S2: Exhaustive search application; Figure S1: Influence of N_{ls}, N_{ts}, and t_s over h_s for each plate configuration; Figure S2: Influence of N_{ls} and N_{ts} over maximum h_s/t_s values for each plate configuration.

Author Contributions: Conceptualization, R.L.V., T.d.S., J.P.S.L. and L.A.I.; methodology, R.L.V., E.D.d.S., L.A.O.R., T.d.S., J.P.S.L. and L.A.I.; software, R.L.V. and G.R.B.; validation, R.L.V. and G.R.B.; formal analysis, R.L.V., T.d.S., J.P.S.L. and L.A.I.; investigation, R.L.V., T.d.S., J.P.S.L. and L.A.I.; resources, E.D.d.S., L.A.O.R. and L.A.I.; data curation, R.L.V. and G.R.B.; writing—original draft preparation, R.L.V. and L.A.I.; writing—review and editing, E.D.d.S., L.A.O.R., T.d.S., J.P.S.L. and L.A.I.; visualization, E.D.d.S., L.A.O.R. and L.A.I.; supervision, J.P.S.L. and L.A.I.; project administration, L.A.I.; funding acquisition, E.D.d.S., L.A.O.R. and L.A.I. All authors have read and agreed to the published version of the manuscript.

Funding: This research was funded by Coordination for the Improvement of Higher Education Personnel (CAPES, funding code 001) and the National Council for Scientific and Technological Development (CNPQ, processes: 307791/2019-0, 308396/2021-9, and 309648/2021-1).

Institutional Review Board Statement: Not applicable.

Informed Consent Statement: Not applicable.

Data Availability Statement: The research data are available in the Supplementary Materials.

Acknowledgments: The authors thank the CAPES and CNPQ for their financial support in the form of doctoral and research productivity scholarships.

Conflicts of Interest: The authors declare no conflicts of interest.

References

1. Tatsumi, A.; Htoo Ko, H.H.; Fujikubo, M. Ultimate strength of container ships subjected to combined hogging moment and bottom local loads, Part 2: An extension of Smith's method. *Mar. Struct.* **2020**, *69*, 102683. [CrossRef]
2. Lee, D.H.; Kee Paik, J. Ultimate strength characteristics of as-built ultra-large containership hull structures under combined vertical bending and torsion. *Ships Offshore Struct.* **2021**, *15* (Suppl. S1), S143–S160. [CrossRef]
3. Ozdemir, M.; Ergin, A.; Yanagihara, D.; Tanaka, S.; Yao, T. A new method to estimate ultimate strength of stiffened panels under longitudinal thrust based on analytical formulas. *Mar. Struct.* **2018**, *59*, 510–535. [CrossRef]
4. Li, D.; Chen, Z.; Chen, X. Numerical investigation on the ultimate strength behavior and assessment of continuous hull plate under combined biaxial cyclic loads and lateral pressure. *Mar. Struct.* **2023**, *89*, 103408. [CrossRef]
5. Ziemian, R. *Guide to Stability Design for Metal Structures*, 6th ed.; Wiley: Hoboken, NJ, USA, 2010.
6. Zhang, D.; Xu, Z.; Okada, T.; Kawamura, Y.; Hayakawa, G.; Ishibashi, K.; Koyama, H. A study on the scantling formulae of a stiffener against lateral pressure under the simultaneous action of axial load. *Mar. Struct.* **2024**, *95*, 103595. [CrossRef]
7. Reis, A.H. Constructal theory: From engineering to physics, and how flow systems develop shape and structure. *Appl. Mech. Rev.* **2006**, *59*, 269–282. [CrossRef]
8. Bejan, A. Constructal-theory network of conducting paths for cooling a heat generating volume. *Int. J. Heat Mass Transf.* **1997**, *40*, 799–816. [CrossRef]
9. Da Silveira, T.; Pinto, V.T.; Lima, J.P.S.; Pavlovic, A.; Rocha, L.A.O.; Dos Santos, E.D.; Isoldi, L.A. Applicability Evidence of Constructal Design in Structural Engineering: Case Study of Biaxial Elasto-Plastic Buckling of Square Steel Plates with Elliptical Cutout. *J. Appl. Comput. Mech.* **2021**, *7*, 922–934.
10. Wang, Z.; Kong, X.; Wu, W.; Kim, D.K. An advanced design diagram of stiffened plate subjected to combined in-plane and lateral loads considering initial deflection effects. *Thin-Walled Struct.* **2024**, *203*, 112144. [CrossRef]
11. Baumgardt, G.R.; Fragassa, C.; Rocha, L.A.O.; Dos Santos, E.D.; Da Silveira, T.; Isoldi, L.A. Computational Model Verification and Validation of Elastoplastic Buckling Due to Combined Loads of Thin Plates. *Metals* **2023**, *13*, 731. [CrossRef]
12. Ma, H.; Xiong, Q.; Wang, D. Experimental and numerical study on the ultimate strength of stiffened plates subjected to combined biaxial compression and lateral loads. *Ocean Eng.* **2021**, *228*, 108928. [CrossRef]
13. Lima, J.P.S.; Cunha, M.L.; dos Santos, E.D.; Rocha, L.A.O.; Real, M.V.; Isoldi, L.A. Constructal Design for the ultimate buckling stress improvement of stiffened plates submitted to uniaxial compressive load. *Eng. Struct.* **2020**, *203*, 109883. [CrossRef]
14. Amaral, R.R.; Troina, G.S.; Fragassa, C.; Pavlovic, A.; Cunha, M.L.; Rocha, L.A.O.; dos Santos, E.D.; Isoldi, L.A. Constructal design method dealing with stiffened plates and symmetry boundaries. *Theor. Appl. Mech. Lett.* **2020**, *10*, 366–376. [CrossRef]
15. Liu, H.; Ong, Y.S.; Cai, J. A survey of adaptive sampling for global metamodeling in support of simulation-based complex engineering design. *Struct. Multidiscip. Optim.* **2018**, *57*, 393–416. [CrossRef]
16. Amouzgar, K.; Strömberg, N. Radial basis functions as surrogate models with a priori bias in comparison with a posteriori bias. *Struct. Multidiscip. Optim.* **2017**, *55*, 1453–1469. [CrossRef]
17. Wang, C.M.; Wang, C.Y.; Reddy, J.N. Exact Solutions for Buckling of Structural Members. In *CRC Series in Computational Mechanics and Applied Analysis*; CRC Press: Boca Raton, FL, USA, 2004. [CrossRef]
18. Przemieniecki. *Theory of Matrix Structural Analysis*; Dover Publications: Mineola, NY, USA, 1985.
19. El-Sawy, K.M.; Nazmy, A.S.; Martini, M.I. Elasto-plastic buckling of perforated plates under uniaxial compression. *Thin-Walled Struct.* **2004**, *42*, 1083–1101. [CrossRef]
20. Fonseca, E.M.M. Steel Columns under Compression with Different Sizes of Square Hollow Cross-Sections, Lengths, and End Constraints. *Appl. Sci.* **2024**, *14*, 8668. [CrossRef]
21. ANSYS Inc. Element reference. In *Ansys Mechanical APDL Manual*; ANSYS Inc.: Canonsburg, PA, USA, 2011.
22. Kim, J.H.; Jeon, J.H.; Park, J.S.; Seo, H.D.; Ahn, H.J.; Lee, J.M. Effect of reinforcement on buckling and ultimate strength of perforated plates. *Int. J. Mech. Sci.* **2015**, *92*, 194–205. [CrossRef]
23. Paik, J.K.; Kim, B.J.; Seo, J.K. Methods for ultimate limit state assessment of ships and ship-shaped offshore structures: Part I-Unstiffened plates. *Ocean Eng.* **2008**, *35*, 261–270. [CrossRef]
24. Paik, J.K.; Kim, B.J.; Seo, J.K. Methods for ultimate limit state assessment of ships and ship-shaped offshore structures: Part II-Stiffened plates. *Ocean Eng.* **2008**, *35*, 271–280. [CrossRef]

25. Beg, D.; Kuhlmann, U.; Davaine, L.; Braun, B. Design of plated structures: Eurocode 3: Design of steel structures. Part 1–5, design of plated structures. In *ECCS—European Convention for Constructional Steelwork*; John Wiley & Sons: Hoboken, NJ, USA, 2010.
26. Suneel Kumar, M.; Lavana Kumar, C.; Alagusundaramoorthy, P.; Sundaravadivelu, R. Ultimate strength of orthogonal stiffened plates subjected to axial and lateral loads. *J. Civ. Eng.* **2010**, *14*, 197–206.